Lipid metabolism of hepatocyte-like cells supports intestinal tumor growth by promoting tracheogenesis

Huang, K.*[1], Miao, T.*[1], Dantas, E.[3,4], Han, M.[1,2], Hu, Y.[1,2], Wang, K.[1], Sanford, J.[3,4], Goncalves, M.[3,4], and Perrimon, N[1,2]

1 Department of Genetics, Blavatnik Institute, Harvard Medical School, Harvard University, Boston, MA 02115, USA
2 Howard Hughes Medical Institute, Boston, MA, USA
3 Division of Endocrinology, Department of Medicine, Weill Cornell Medicine, New York, NY 10065, USA.
4 Meyer Cancer Center, Weill Cornell Medicine, New York, NY 10065, USA.

^Correspondence:
Kerui Huang: Kerui_Huang@hms.harvard.edu
Norbert Perrimon: perrimon@genetics.med.harvard.edu

*Authors contribute equally

Abstract

Tumors require metabolic adaptations to support their rapid growth, but how they influence lipid metabolism in distant tissues remains poorly understood. Here, we uncover a novel mechanism by which gut tumors in adult flies reprogram lipid metabolism in distal hepatocyte-like cells, known as oenocytes, to promote tracheal development and tumor growth. We show that tumors secrete a PDGF/VEGF-like factor, Pvf1, that activates the TORC1-Hnf4 signaling pathway in oenocytes. This activation enhances the production of specific lipids, including very long-chain fatty acids and wax esters, that are required for tracheal growth surrounding the gut tumor. Importantly, reducing expression in oenocytes of either the transcription factor *Hnf4*, or the elongase mElo that generates very long chain fatty acid suppresses tumor growth, tracheogenesis, and associated organ wasting/cachexia-like phenotypes, while extending lifespan. We further demonstrate that this regulatory pathway is conserved in mammals, as VEGF-A stimulates lipid metabolism gene expression in human hepatocytes, and lung tumor-bearing mice show increased hepatic expression of *Hnf4* and the lipid elongation gene *Elovl7*. Our findings reveal a previously unrecognized tumor-host interaction where tumors non-autonomously reprogram distal lipid metabolism to support their growth. This study not only identifies a

36 novel non-autonomous role of the TORC1-Hnf4 axis in lipid-mediated tumor progression
37 but also highlights potential targets for therapeutic intervention in cancer-associated
38 metabolic disorders.
39
40 **Introduction**
41 Tumor growth demands a growing supply of nutrients and oxygen. The growing
42 tumor constantly shapes its microenvironment to favor fast growth and expansion, through
43 secreted factors and extracellular matrix. The composition of the tumor microenvironment
44 (TME) varies between tumor types, but the hallmarks include increased blood vessels,
45 immune cells, stromal cells, and extracellular matrix [1]. To overcome the increasingly
46 hypoxic and acidic environment, TME promotes angiogenesis to restore oxygen and
47 nutrient supply. In addition to modulating the local TME, malignant cells can exert systemic
48 effects on distant organs—including the liver, skeletal muscle, and brain—to reshape the
49 host's metabolic pathways, ultimately promoting further tumor progression [2-6]. Liver is a
50 metabolic center for amino acids, carbohydrates, and lipid. A key liver-specific metabolic
51 function is the complete urea cycle (UC), which eliminates excess ammonia by converting
52 into urea, a less toxic waste. Previous studies have identified evidence of decreased UC
53 activity in the livers of 4T1 breast cancer bearing mice, and the plasma of children with
54 cancer [5], demonstrating an existing interaction between tumors and the liver. Delineating
55 molecular pathways involving tumor-host interaction can provide novel therapeutic targets.
56 Lipids play a critical role in cancer progression, by serving as building blocks, energy
57 sources and signaling molecules. It has been observed that tumor cells reprogram lipid
58 metabolism to enhance growth, characterized by increased lipid synthesis, lipid uptake,
59 fatty acid oxidation (FAO) and lipid storage [7]. Tumor cells also actively reshape lipid
60 metabolism in cells from the TME through secreted signaling molecules and drive TME to
61 favor tumor growth. For example, increased lipid uptake and FAO in regulatory T cells
62 (Tregs), tumor-associated macrophages (TAMs) and myeloid-derived suppressor cells
63 (MDSCs), promotes their immunosuppressive function [8-10]. However, whether tumor

64 cells also reshape lipid metabolism in distal organs, such as liver, which is a metabolic
65 center for lipid transport, is not known.
66 To better understand the reciprocal communication between liver and tumor cells,
67 we utilize *Drosophila* which has emerged as a simple yet powerful model to study tumor-
68 host interactions [11]. The fly midgut, oenocytes, fat body and malpighian tubules are
69 functionally equivalent to human digestive tract, hepatocytes, adipose tissue and kidney,
70 respectively [12]. Oenocytes, which are hepatocyte-like cells, are important for mobilizing
71 stored lipids during starvation and interact closely with metabolic tissues, such as the fat
72 body to regulate lipid uptake and reprocessing [13, 14]. In addition to regulating lipid
73 metabolism under nutritional deprivation, oenocytes are the major site for synthesis of
74 cuticular hydrocarbons in pterygote insects [15-17]. Adult oenocytes synthesize
75 hydrocarbons using fatty acyl-CoA precursors via reduction to fatty aldehyde and oxidative
76 decarbonylation [18, 19]. Many fatty acid synthases, elongases and desaturases expressed
77 in adult oenocytes produce various types of fatty acyl-CoA substrates that are processed to
78 form a complex blend of cuticular hydrocarbons [20-23]. Hepatocyte nuclear factor 4
79 (Hnf4), an oenocyte enriched transcription factor, plays an important role in regulating the
80 conversion of lipids to very long chain fatty acid, which are important substrates for
81 hydrocarbon synthesis [23]. Oenocytes are the major site for lipid transport and
82 processing, reminiscent of human hepatocytes. However, whether and how oenocytes
83 regulate tumor growth is unknown.
84 The *Drosophila* trachea is a network of oxygen transporting tubes, the functional
85 equivalent of mammalian blood vessels [24]. Trachea is composed of terminal tracheal
86 cells (TTCs), which are highly plastic cells, and the terminal branches (TBs) or tracheoles
87 which deliver oxygen to the tissues. TTCs are oxygen sensing cells, and hypoxic conditions
88 promote the formation of TBs through hypoxia-inducible factor-1α (HIF-1α; Similar (Sima)
89 in *Drosophila*), similar to the role of HIF-1α in mammalian angiogenesis. Trachea resides in
90 proximity of many tissues, including the midgut. Trachea penetrate the visceral muscles to
91 access the intestinal epithelium to supply it with oxygen [25]. The intestinal epithelium is
92 apicobasally polarized, composed of intestinal stem cells (ISCs) and their progeny.

93 Damage induced by enteric infection, oxidative agents and tumor growth can increase
94 tracheogenesis on the midgut, which is necessary for efficient damage-induced ISC-
95 mediated regeneration [26, 27]. Additionally, tumor-induced tracheogenesis in *Drosophila*
96 is reminiscent of cancer-induced angiogenesis in mammals [26].
97 Using a Drosophila gut tumor model, we uncover a novel mechanism through which
98 gut tumors reprogram lipid metabolism in distal oenocytes to promote both tracheal
99 development and tumor growth. We find that tumors secrete a PDGF/VEGF-like factor,
100 Pvf1, which activates the TORC1-Hnf4 signaling pathway in oenocytes. This activation
101 boosts the production of specific lipids, including very long-chain fatty acids and wax
102 esters, essential for tracheal growth around the tumor. Notably, reducing the activity of
103 Hnf4 and mElo, an elongase involved in generating very long-chain fatty acids, in oenocytes
104 suppress tumor growth, tracheal development, and cachexia-like phenotypes, while also
105 extending lifespan. Additionally, we demonstrate that this regulatory pathway is conserved
106 in mammals, as VEGF-A stimulates lipid metabolism gene expression in human
107 hepatocytes, and tumor-bearing mice exhibit increased hepatic expression of lipid
108 elongation genes. Our findings highlight a previously unrecognized tumor-host interaction,
109 where tumors non-autonomously reprogram distal lipid metabolism to facilitate their
110 growth.
111
112 **Results**
113 ***Oenocyte lipid metabolism regulated by Hnf4 controls tumor proliferation***
114 To investigate how tumor growth rewires lipid metabolism of the whole fly, we
115 expressed an active form of *Yorkie (yki^{3SA}),* in adult gut stem cells, using the intestinal stem
116 cells (ISCs)/enteroblast driver (*Esg-Gal4* or *Esg-LexA*), hereafter referred to as Yki flies [28].
117 *Esg-Gal4* or *Esg-LexA* was combined with the *tubulin* promoter-driven temperature-
118 sensitive *GAL80 (tubP-GAL80^{TS}),* to control the temporal expression of Gal4 or LexA. Next,
119 we conducted untargeted lipidomic profiling using an LC-MS/MS-based platform of whole-
120 body samples of adult female flies (*Esg-LexA > LexAop-yki^{3SA}*) expressing *yki^{3SA}* for 3 days,
121 together with control flies (*Esg* > +). The complete *Drosophila* genotype information can be

122 found in Supplementary Table 1. Female flies are used in the analysis unless otherwise
123 noted, because they show more significant and consistent tumor-associated cachexia
124 phenotypes. We detected 2471 lipid species in total representing 45 lipid classes
125 (Supplementary Table 2). The lipidomic analysis showed an increase in wax ester (WE),
126 monogalactosyldiacylglycerol (MGDG), phosphatidylglycerol (PG), phosphatidylcholine
127 (PC), and ceramide (Cer) level in Yki flies (Figure 1A). We also observed a slight reduction of
128 triglycerides (TG) levels in Yki flies at early stage, in agreement with previous findings [29].
129 WEs are major components of cuticular lipids, which cover nearly all parts of terrestrial
130 arthropods [30] to restrict water loss, and WE levels are significantly increased in Yki flies
131 (Figure 1B), yet the significance of this regulation is unknown. As the biosynthesis of
132 cuticular lipids mainly occurs in *Drosophila* oenocytes and Hnf4 is a main regulator of this
133 process [23], we tested whether oenocyte Hnf4 regulates the level of WEs in wild type flies.
134 WEs were reduced when *Hnf4* was knocked down in wild type adult oenocytes using the
135 *PromE(800)-Gal4* Gene-switch driver (hereafter referred to as PromE^{gs}) [14], where the
136 driver is activated upon mifepristone feeding (RU) (Figure 1C). Next, to test whether Hnf4
137 regulates WE synthesis in Yki flies, we used the LexA-LexAop system to induce Yki tumors
138 in the gut and the Gal4/UAS system combining GAL80 in oenocytes (*PromE-GAL4,Tub-*
139 *GAL80^{TS}*, referred to as *PromE*) to knockdown *Hnf4*. Knockdown of *Hnf4* in oenocytes
140 decreased Yki-induced WE levels (Figure 1D), indicating that *Hnf4* expression in oenocytes
141 is required for the increase of WE level in Yki flies.
142 As a nuclear receptor, the localization of Hnf4 is highly enriched in oenocyte nuclei
143 compared to the fat body [23, 31]. To visualize the localization of Hnf4, we tagged the
144 endogenous *Hnf4* gene with 127D01, a small epitope tag that can be detected with a
145 specific nanobody [32, 33], using an homology directed repair pathway CRISPR-Cas9
146 targeted insertion method [32]. To validate the Hnf4-127D01 line, we knocked down *Hnf4* in
147 oenocytes (Figure S1A), which significantly reduced its nuclear localization (Figure S1B).
148 Hnf4-127D01 in wild type oenocytes showed high level of nuclear localization, consistent
149 with previous findings (Figure 1E) [31]. Interestingly, increased nuclear localization of Hnf4-
150 127D01 was observed in the oenocytes of Yki flies (Figure 1E-1F). Altogether, these data

151 suggest that oenocytes in Yki flies have increased Hnf4 activity. To test whether oenocyte
152 Hnf4 signaling is required for tumor growth, we measured ISC-mitosis using phospho-
153 histone 3 (pH3+) staining. Inhibition of *Hnf4* in oenocytes of Yki flies *(Esg-LexA>yki^{3SA};*
154 *PromE>Hnf4-i)* for 3 days showed a decrease in pH3+ staining compared to controls (*Esg>*
155 *UAS-yki^{3SA}*), and a slower growth rate for tumor (Figure 1G). Importantly, knockdown of *Hnf4*
156 alone in wild type animals does not affect pH3+ number compared to control (Figure 1G),
157 indicating that the role of Hnf4 in Yki flies relates to the aberrant regulation of Hnf4 in Yki
158 flies. In wild type flies, knocking down *Hnf4* in oenocytes for 7 days resulted in a slight
159 reduction in ovary size (Figure S1C-D), suggesting long-term reduction of *Hnf4* is
160 detrimental to the ovary development. Further, oenocyte *Hnf4* knockdown in Yki flies for 3
161 days could rescue the level of both ovary wasting, bloating and induced wet weight (Figure
162 1H-1I, Figure S1E), indicating that aberrant Hnf4 activity in oenocytes contribute to tumor
163 growth and associated cachexia phenotypes.
164 Our result suggests that Hnf4 transcriptional activity is induced in Yki oenocytes. To
165 validate this, we measured whether the expression of Hnf4 targets in Yki oenocytes also
166 increased. Published studies identify that Hnf4 target genes are involved in beta-oxidation
167 and very long chain fatty acid (VLCFA) biosynthesis in oenocytes [23, 34], we tested
168 whether VLCFA biosynthesis genes (*Hnf4, mElo, CG30008, CG16904, FarO, ACC, HDAC,*
169 *TER, Cyp4g1, Cpr*), as well as genes involved in beta-oxidation (*Whd, Scu, Yip2* and
170 *CG7461)* were dysregulated in Yki flies. *CG30008, CG16904, FarO, ACC, HDAC, TER,*
171 *Cyp4g1, Cpr, Whd, Scu, Yip2* showed no difference between control and Yki flies (Figure
172 S1F). However, we observed a significant increase in *mElo* (Figure 1K), which encodes a
173 methyl-branched cuticular hydrocarbon elongase [21] and a minor increase for *Hnf4 and*
174 *CG7461* (Figure S1F).
175 *mElo* has recently been shown to produce long chain methyl-branched cuticular
176 hydrocarbons in oenocytes that help prevent desiccation [21], a key function of *Hnf4* in
177 oenocytes [23]. Additionally, *mElo* expression is highly enriched in wild type adult
178 oenocytes according to snRNAseq data (Figure 1L). Inhibition of *Hnf4* reduced *mElo*
179 expression, and overexpression of *Hnf4* led to increased levels of *mElo* (Figure S1G-H),

180 consistent with a previous report that mElo is a transcriptional target of *Hnf4* [23]. Further,
181 *mElo* is highly induced in the oenocytes of Yki flies and this induction is blocked when *Hnf4*
182 is knocked down (Figure 1K).
183 In wild type flies, reduction of *mElo* in oenocytes did not affect pH3+ number in the
184 gut (Figure 1M). To test the function of oenocyte *mElo* during tumor growth, we reduced the
185 level of oenocyte *mElo* in Yki flies and observed fewer pH3+ in the gut, suggesting that *mElo*
186 contributes to Yki tumor growth (Figure 1M). We validated the effectiveness of *mElo*
187 knockdown in the oenocytes (Figure S1I). Unlike *Hnf4,* reducing *mElo* expression in wild
188 type oenocytes did not cause steatosis and a reduction of ovary size, suggesting that other
189 targets of *Hnf4* regulate oenocytes steatosis and ovary size (Figure 1N and Figure S1J-S1K).
190 Consistently, *mElo* knockdown did not rescue ovary wasting in Yki flies (Figure S1L).
191 To assess whether oenocyte lipid metabolism affects the viability of Yki flies, we
192 inhibited *Hnf4* in oenocytes and observed a significant lifespan extension (Figure 1O).
193 Inhibition of mElo in oenocytes of Yki flies also significantly increased lifespan (Figure 1P).
194 Finally, *mElo* has a sex specific function in regulating different types of hydrocarbons [21].
195 Therefore, we tested whether *mElo* also regulates Yki viability in male flies. Strikingly,
196 inhibition of *mElo* also significantly increased the lifespan in Yki males (Figure S1M).
197
198 ***Oenocyte Hnf4 activity is regulated by TORC1***
199 We next sought to determine the factors regulating Hnf4 level in oenocytes. Previous
200 studies have shown that inhibiting the TORC1 pathway in oenocytes leads to steatosis [35],
201 a phenotype that mimics reduced Hnf4 expression in these cells [23], suggesting that the
202 TORC1 pathway positively regulates Hnf4 transcription in oenocytes. The Tuberous
203 Sclerosis Complex (TSC) is known to negatively regulate TORC1 by inhibiting RAS homolog
204 enriched in brain (Rheb) activity [36]. Using a previously published snRNAseq dataset [35],
205 we found that overexpression of Tsc1 together with Tsc2 (TSC1,2) in oenocytes, which
206 inhibits TORC1, resulted in reduced Hnf4 expression specifically in oenocytes (Figure 2A),
207 but not in muscle nor fat body tissues, suggesting that that TORC1 positively regulates Hnf4
208 level in oenocytes.

209 Next, we examined the protein level of endogenously tagged Hnf4-127D01 following
210 *TSC1,2* over-expression and observed a significant reduction in Hnf4-127D01 levels in
211 oenocytes, particularly in the nucleus as Hnf4 is a transcription factor (Figure 2B-C). Given
212 that Hnf4 regulates hydrocarbon synthesis in oenocytes and its knockdown increases the
213 susceptibility to dry starvation [23], we overexpressed *TSC1,2* in oenocytes and found that
214 it led to an increased sensitivity of flies to dry starvation (Figure S2A). Additionally, as Hnf4
215 regulates the expression of genes involved in very-long-chain fatty acid (VLCFA) synthesis
216 [23], we analyzed the expression of VLCFA synthesis genes in snRNAseq data from control
217 (*PromE>EGFP*) versus TSC1,2-overexprerssing oenocytes (*PromE>TSC1,2*). Using uniform
218 Manifold Approximation and Projection (UMAP), which identifies cell types in mixed
219 populations based on snRNAseq data, we found that VLCFA synthesis genes were highly
220 enriched in oenocytes (Figure 2D). The ModuleScore, calculated by averaging the
221 expression of the VLCFA synthesis pathway genes and subtracting the expression of a
222 randomly selected gene set expression, decreased in oenocytes upon *TSC1,2*
223 overexpression (Figure 2D).
224 Inhibition of TORC1 through overexpressing *TSC1,2,* or overexpressing Proline-rich
225 Akt substrate 40 kDa (*PRAS40)*, or by feeding flies with rapamycin, all induced steatosis in
226 oenocytes (Figure 2E and S2B-C), as observed following *Hnf4* knockdown in oenocytes
227 (Figure 1N). However, simultaneous overexpression of *Hnf4* with *TSC1*,2 prevented the
228 development of steatosis (Figure 2E), indicating that TORC1 regulates oenocyte lipid
229 metabolism via Hnf4. Lastly, *TSC1,2* overexpression also reduced the expression of *mElo*
230 and *FASN2,* which are Hnf4 target genes, and overexpressing *Hnf4* simultaneously blocked
231 this decrease (Figure 2F-G). Together, these findings suggest that Hnf4 acts downstream of
232 TORC1 to regulate lipid metabolism in oenocytes.
233 Next, we also tested the effects of oenocyte *TSC1,2* in tumor growth. Consistent
234 with *Hnf4* and *mElo* knockdown, *TSC1,2* overexpression in oenocytes reduced tumor
235 induced WE levels (Figure 2H). We also observed an increased level of TORC1 activity, as
236 measured by phospho-4EBP (p4EBP) staining in oenocytes of Yki flies (Figure 2I-J).
237 Additionally, overexpressing *TSC1,2* blocked *mElo* expression in oenocytes of Yki flies

238 (Figure 2K), Yki-induced pH3^{+} cells in the gut (Figure 2L), as well as Yki-induced ovary
239 wasting and bloating (Figure 2M and S2D). Altogether, these results indicate that TORC1
240 regulate Hnf4 transcription and protein level in oenocytes and its activation is required for
241 tumor growth.
242
243 ***ISCs secreted Pvf1 regulates Hnf4 through PvR signaling in oenocytes and affects***
244 ***tumor associated phenotypes***
245 TORC1 activity is regulated through various pathways, one of which includes
246 PDGF/VEGF signaling. Studies have shown that PvR activation can stimulate the TOR
247 pathway [35, 37, 38]. Consistent with this, muscle-secreted Pvf1 can regulate TORC1
248 activity in the oenocytes [35], suggesting that the activation of the TORC1-Hnf4 axis in
249 oenocytes of Yki flies may occur through PvR activation. Yki-expressing ISCs are capable of
250 secreting higher levels of the Pvf1 ligand, which activates PvR signaling in surrounding
251 tissues [39]. However, *Pvf1* is expressed at low levels in oenocytes and is not significantly
252 induced in Yki flies (Figure S3A-C). To test whether ISC secreted Pvf1 can induce oenocyte
253 Hnf4 levels, we overexpressed *Pvf1* specifically in adult ISCs (*Esg>Pvf1*) and measured
254 Hnf4-127D01 nuclear level in oenocytes. *Pvf1* overexpression in ISCs increased nuclear
255 Hnf4-127D01 levels (Figure 3A-B), suggesting an increased transcriptional activity as
256 measured by increased level of *mElo* expression (Figure 3C). To test whether ISC-derived
257 Pvf1 activates PvR in oenocytes, we overexpressed an active form of PvR in oenocytes
258 which was associated with increased nuclear Hnf4-127D01 level, as well as increased level
259 of *mElo* expression (Figure 3D-F). To determine whether tumor secreted Pvf1 non-
260 autonomously activates Hnf4 level in oenocytes, we knocked down *Pvf1* expression in the
261 ISCs of Yki flies (*Esg>yki^{3SA}; Pvf1-i*) and observed its effect on Hnf4-127D01 nuclear level.
262 *Esg>yki^{3SA}; Pvf1-i* significantly reduced the level of Hnf4-127D01 nuclear localization
263 compared to *Yki* flies (*Esg>yki^{3SA}; Luc-i)* (Figure 3G-H). Consistently, *mElo* expression was
264 reduced in *Esg>yki^{3SA}; Pvf1-i* flies compared to Yki flies (Figure 3I). We also tested whether
265 Pvf1 reduction in Yki flies would affect tumor development, like Hnf4 inhibition in
266 oenocytes. As reported previously [39], inhibition of *Pvf1* in the tumor gut rescues both

267 bloating and ovary wasting (Figure 3J-K). Gut tumors in *Esg>yki^{3SA};Pvf1-i* flies exhibited
268 slower growth at early stage, as shown by reduced number of pH3+ cells (Figure 3L).
269 Finally, to demonstrate that Pvf1 secreted from Yki tumors directly controls *mElo*
270 expression through PvR, we used the dual Gal4 and LexA systems to reduce *PvR* level in
271 oenocytes while inducing Yki in ISCs. *Esg-LexA>yki^{3SA};PromE>PvR-i* animals showed
272 reduced *mElo* expression (Figure 3M), decreased the level of bloating and ovary wasting,
273 reduced the number of pH3+ cells in gut tumors (Figure 3N-P), and extended lifespan,
274 compared to Yki flies (Figure 3Q). Altogether, these data suggests that PDGF/VEGF induced
275 by Yki tumor non-autonomously increases Hnf4 activity in oenocytes through PvR.
276
277 ***Circulating lipids target trachea but not ISCs to promote trachea growth***
278 To identify the lipid species induced by oenocytes in Yki flies, we performed
279 lipidomic analysis on the fly hemolymph of control flies, *Esg-LexA> yki^{3SA}* and *Esg-LexA>*
280 *yki^{3SA}; PromE>Hnf4-i* flies (Figure 4A, Supplementary Table 3). Among the lipid species that
281 are induced by Yki and decreased by *Esg-LexA > yki^{3SA}; PromE>Hnf4-i*, the majority are
282 phospholipids including phosphotidyl choline (PC), phosphatidylglycerol (PG) and
283 phosphatidylethanolamine (PE), triglycerides (TGs) and acylcarnitines (AcCas). More
284 specifically, AcCa 24:1 and AcCa 24:2, which are long-chain acylcarnitines (C≥12)
285 secreted by mitochondria when metabolism is inhibited [40], were elevated in Yki flies
286 while reduced by *Hnf4* knockdown (Figure 4B-C). Circulating PC 36:4, and PE 32:5
287 phospholipids and TG(18:3_16:0_16:1), TG(18:2_16:0_18:0) triglycerides were induced in
288 Yki flies and rescued by *Hnf4* knockdown (Figure 4D-G). Interestingly, PC 36:4 is elevated in
289 the serum and plasma samples from breast cancer patients [41] and TG(18:2_16:0_18:0) is
290 induced in bladder cancer patients [42].
291 PC and PE are the most abundant phospholipids of cellular membranes and play
292 important role in lipoprotein metabolism. In insects, lipid transport in circulation relies on
293 lipophorins, which are the major lipoproteins. The increased circulation of PC 36:4 and PE
294 32:5 in Yki flies suggests an increase in lipoproteins that transport lipids from oenocytes
295 towards trachea or the midgut.

296 The transport of lipids, such as phospholipids from oenocytes, to the trachea or
297 ISCs to promote tumor growth has not been reported [26]. Thus, we inhibited Hnf4 activity
298 in oenocytes by overexpressing *TSC1,2*, knocking down or overexpressing *Hnf4*, and
299 observed no significant effect on the number of pH3+ cells in the midgut (Figure 4H). Since
300 95% of the hemolymph lipids are transported through lipophorin (Lpp) in flies [43], and that
301 low-density lipoprotein (LDL) receptor homologues LpR1 and LpR2 promote Lpp
302 internalization [44], we reduced LpR1 or LpR2 level in the ISCs. However, this had no
303 impact on the trachea area, skeleton length, and only a minor increase in the number of
304 branches in the *LpR1* knockdown condition (Figure S4A-C). Reducing LpR1 and LpR2
305 activities in the ISCs also did not affect the proliferation (Figure S4D). To further examine
306 the role of LpR1 or LpR2 in ISC tumors, we reduced LpR1 and LpR2 levels while
307 overexpressing Yki (*Esg> yki^{3SA};LpR1-i and Esg> yki^{3SA};LpR2-i*), and found that these
308 manipulations did not impair Yki-induced tracheal growth (Figure 4I-K) or prevent Yki-
309 induced ISC proliferation (Figure 4L). These results suggest that ISC proliferation does not
310 rely on circulating lipids in the hemolymph.
311 We further tested whether disrupting *LpR1* and *LpR2* activities in trachea could
312 blunt tracheal growth. Knocking down *LpR1* using a temperature sensitive trachea-specific
313 driver (*btl-GAL4, UAS-srcGFP, Tub-GAL80^{TS},* referred to as *Btl*) reduced tracheal number of
314 branches, tube area and skeleton length compared to control flies (*Btl*>+), whereas
315 knocking down *LpR2* in trachea did not have a significant effect (Figure 4M-O). Reducing
316 LpR1 and LpR2 activities in the trachea did not affect ISC proliferation (Figure S4E). This
317 suggests that trachea growth, but not ISC growth, requires lipids generated from oenocytes
318 transported through lipophorins.
319
320 ***Oenocyte Hnf4 and mElo regulates tracheogenesis in the midgut***
321 Next, we aimed to understand whether oenocyte lipid metabolism controls trachea
322 growth in wild type guts. Consistent with Hnf4 knockdown, oenocyte specific *mElo*
323 reduction and *TSC1,2* overexpression showed reduced level of whole body WE in non-Yki
324 flies (Figure 5A-B). WEs are essential parts of the outer layer of the trachea [45-48], and

325 *waterproof* (*wat*), which is involved in biosynthesis of wax, has been implicated in
326 hydrophobic tracheal coating in *Drosophila* embryos [48]. Knocking down *Hnf4* did not
327 affect the transepithelial barrier mediated by septate junctions in the midgut trachea on the
328 midgut, as revealed by red dextran injection experiment (Figure 5C). However, reduction of
329 oenocyte *Hnf4* altered the morphology of trachea associated with the midgut (R2-R4
330 regions) (Figure 5D). Specifically, we observed a reduction in the number of branches and
331 total skeleton length, normalized to the area of the gut surface (Figure 5E-G). Consistently,
332 we also observed a reduction in branch numbers, tube area and skeleton length when
333 *mElo* was knocked down in oenocytes of wild type flies (Figure 5H-J). The effect of oenocyte
334 Hnf4 on trachea number is not specific to the midgut, as we also observed a reduction of
335 trachea total tube area in the ovary of wild type flies (Figure S5A-D). Overexpressing *Hnf4* or
336 *mElo* is sufficient to induce total tracheal tube area and skeleton length in the midguts of
337 wild type flies (Figure 5K-P). Finally, to eliminate the effect of RU feeding on trachea
338 morphology, we fed control (*PromE>ctrl*) flies and observed no difference in trachea
339 morphology (Figure S5E-G).
340

341 ***Hnf4-mElo axis in oenocytes mediates lipid metabolism and tracheogenesis***
342 ***induced by Yki tumors***

343 Tumor growth in the adult *Drosophila* midgut has been previously shown to promote
344 tracheole density [26]. Similarly, we observed an increase in the number of trachea
345 branches, total tube area, and total tube length in the surrounding tissue of the Yki midgut
346 (Figure S6A-D). This led us to investigate whether oenocyte lipid metabolism mediated by
347 *Hnf4-mElo* axis is crucial for trachea growth in the Yki midgut. Our lipidomic analysis
348 showed reduced whole body WE level when *Hnf4* is knocked down, or when *TSC1*,2 is
349 overexpressed in the oenocytes of Yki flies (Figure S6E).

350 To explore whether perturbations of lipid metabolism in oenocytes could block Yki-
351 induced tracheogenesis in the midgut, we manipulated lipid metabolism by overexpressing
352 TSC1,2 or knocking down Hnf4 or mElo. Using the LexA/LexAop and Gal4/UAS systems, we
353 found that overexpressing TSC1,2 or reducing mElo significantly decreased the number of

354 tracheal branches, total tube area, and total tube length in the Yki midgut. Reducing Hnf4
355 levels, on the other hand, only decreased the total tube area (Figure 6A-C).
356 In addition, to verify whether midgut secreted Pvf1 regulates tracheal growth, we
357 knocked down *Pvf1* in ISC in addition to Yki overexpression. Reduction of *Pvf1* blocked Yki
358 induced number of branches, tube area and skeleton length (Figure 6D-F), indicating that
359 oenocyte lipid metabolism is important for trachea growth induced by Yki.
360
361 ***Regulation of hepatocyte lipid metabolism by pro-angiogenic factors in tumor models***
362 Using the *Drosophila* Yki tumor model, we found that the tumor secreted
363 PDGF/VEGF-like factor Pvf1 can non-autonomously regulate Hnf4 activity in hepatocyte-
364 like cells to promote the production of VLCFA or related lipids. To test whether this
365 mechanism is conserved in mammals, we incubated HepG2 cells with vascular
366 endothelial growth factor A (VEGF-A), which is orthologous to Pvf1 in flies and a potent pro-
367 angiogenic growth factor expressed in many types of tumors. We measure the expression
368 level of ELOVL fatty acid elongase 1 – 7 (*ELOVL1-7*). Incubating HepG2 with VEGF-A for 24
369 hours can significantly increase the level of *ELOVL1, 2, 4, 6* and *7*, suggesting a conserved
370 regulation of PDGF/VEGF on lipid metabolism in hepatocytes (Figure 7A-E). In addition, we
371 collected liver samples from *KrasG12D/+;Lkb1f/f* (KL) mice, in which tumors were
372 specifically induced in the lungs, and analyzed the expression levels of *Hnf4a* and *Elovl1-7*
373 in the hepatocytes. *Hnf4a* and *Elovl7* showed higher expression level in the tumor bearing
374 mice, compared to control, suggesting that tumor growth in the lung increased the level of
375 genes involved in lipid metabolism in distal hepatocyte tissues in the KL mouse model
376 (Figure 7F-G). Altogether, these data showed that a conserved mechanism of PDGF/VEGF-
377 like factor in regulating VLCFA metabolism in hepatocytes through Hnf4.
378
379 **Discussion**
380 We reveal a novel mechanism by which gut tumors in Drosophila reprogram lipid
381 metabolism in oenocytes to promote tracheal development and tumor growth. Our
382 findings demonstrate that tumors secrete a PDGF/VEGF-like factor, Pvf1, which activates

383 TORC1 activity, triggering the expression of mElo through Hnf4 in oenocytes. This TORC1-
384 Hnf4 signaling pathway enhances the production of specific lipids, such as very long-chain
385 fatty acids and wax esters, which stimulate tracheal growth, a crucial process for tumor
386 expansion. We also show that reducing Hnf4 or mElo activity in oenocytes suppresses
387 tumor growth, tracheogenesis, and tumor-induced cachexia, while extending lifespan.
388 Additionally, we highlight the conservation of this regulatory pathway in mammals, where
389 VEGF-A stimulates lipid metabolism gene expression in human hepatocytes. Furthermore,
390 lung tumor-bearing mice exhibit increased Hnf4 and Elovl7 expression in peripheral
391 hepatocytes.

392 Pvf1, a tumor-secreted factor, has previously been linked to tumor-induced muscle
393 and fat body wasting, as well as renal dysfunction in *Drosophila* [39, 49, 50]. In this study,
394 we uncover a novel role for tumor-secreted Pvf1 in modulating oenocyte lipid metabolism
395 through TORC1 and Hnf4, which regulates the expression of the oenocyte-enriched gene
396 mElo (Figure 3). While Hnf4 activity is known to be induced by starvation and during the
397 developmental transition from pupae to larvae [23, 34], its upstream regulators remain
398 poorly understood. In MEF cells, the Hnf4 binding motif is highly enriched in the promoters
399 of TORC1-induced genes [51], suggesting Hnf4α mediates the transcriptional activities of
400 TORC1. Here, we demonstrate that TORC1 positively regulates Hnf4 protein levels in the
401 oenocyte nucleus through transcriptional regulation (Figure 2A). However, the precise
402 mechanisms controlling *Hnf4* transcription downstream of TORC1 remain unclear. REPTOR
403 and REPTOR-BP are likely key players in this process, as they are the major effectors of the
404 transcriptional response induced by TORC1 inhibition [52].

405 Our study identified a novel mode of communication between oenocytes and the
406 gut. Oenocytes produce lipid substrates that support gut tracheal growth, a process crucial
407 for tumor expansion and potentially ISC growth. Similar to tumor, bacterial infections and
408 epithelial damage also trigger ISC proliferation [53-55], suggesting that oenocyte-secreted
409 lipids may also support stress-induced ISC expansion. We found that lipids from oenocytes
410 are acquired by the tracheal cells instead of ISCs, as knockdowns of *LpR1* and *LpR2* in ISCs
411 have no effects in tumor growth (Figure 5I-L). In contrast, reducing *LpR1* in tracheal cells

412 was sufficient to decrease tracheal development (Figure 5M-O). This may be due to the
413 trachea's direct contact with hemolymph, allowing it to actively acquire lipids, while the
414 midgut is covered by visceral muscle and basement membrane [56, 57].
415 The mechanism by which VLCFA metabolism regulates tracheogenesis remains
416 unclear, though it may involve the induction of Reactive Oxygen Species (ROS) in the
417 trachea. ROS has been implicated in the activation of HIF-1α/Sima, and that VLCFAs is
418 known to induce mitochondrial dysfunction and ROS production [58-60]. Increased ROS
419 levels, through treatments such as paraquat, H_2O_2 or bacterial infection, have been shown
420 to induce tracheogenesis in the midgut [26]. Furthermore, manipulating ROS level in the
421 trachea alone can trigger tracheal branching and ISC proliferation [26]. Interestingly,
422 overexpressing *Hnf4* alone in oenocytes could promotes tracheogenesis, but does not
423 significantly induce ISC proliferation (Figure 4H). This difference may be attributed to
424 variations in driver strength, with tracheal development occurring prior to ISC proliferation.
425 We observed that VEGF-A stimulates lipid metabolism gene expression in human
426 hepatocytes, and lung tumor-bearing mice showed increased expression of *Hnf4* and
427 *Elovl7* in peripheral hepatocytes. This work provides new insights into tumor-host
428 interactions, challenging the conventional view that tumor-associated metabolic changes
429 are merely passive processes and instead demonstrating their role in promoting tumor
430 growth. Specifically, inhibiting *Hnf4* and *mElo* in oenocytes slows tumor growth, halts
431 tumor-induced cachexia, and extends the lifespan of flies (Figures 1N, 1P, and S1M). Yki
432 activation increased levels of AcCas, PCs, and TAGs in the hemolymph, and inhibiting *Hnf4*
433 in oenocytes reversed these lipid changes induced by Yki (Figure 4A). This study identifies
434 the TORC1-Hnf4-Elovl7 axis and tumor-induced lipid metabolism as potential therapeutic
435 targets for managing tumor growth or as biomarkers for early tumor detection.
436 Hnf4 is a master regulator of multiple metabolic pathways in *Drosophila* and
437 inhibiting it could have broad effects on the host. For instance, knocking down *Hnf4* in non-
438 tumor-bearing flies led to increased steatosis and smaller ovaries (Figures 1N, S1C-D).
439 These wide-ranging effects may limit the efficacy of Hnf4 inhibition as an anti-tumor
440 strategy. In contrast, mElo, which is more specifically involved in lipid elongation, presents

441 a more targeted inhibition with lower toxicity and a greater extension of lifespan (Figures 1P,
442 S1M). Our study also suggests a potential role for elongases in tumor-induced
443 angiogenesis, as overexpression of ELOVL7 has been linked to prostate cancer and is
444 required for cancer growth [61]. While mElo is exclusively expressed in oenocytes in flies
445 (Figure 1L), its orthologue, ELOVL7, is widely expressed in multiple tissues, including the
446 prostate, kidney, brain, small intestine, and thyroid [62]. It is plausible that ELOVL7 is
447 upregulated in various tissues in cancer patients, indicating additional tissue targets for
448 anti-angiogenic therapies.
449 In summary, our data reveal a novel paradigm in which growing tumors actively
450 acquire substrates for tracheogenesis by secreting a PDGF/VEGF-like factor that activates
451 the TORC1-Hnf4 axis in distal oenocytes, inducing the expression of mElo. This promotes
452 the synthesis of VLCFAs, which are transported to the trachea to further support tumor
453 growth (Figure 7H).
454
455 **Materials and Methods**
456 ***Drosophila stocks and husbandry***
457 All experiments were conducted using female flies due to their more consistent
458 bloating phenotype and larger oenocyte, which facilitated dissection. For temperature-
459 sensitive experiments, fly crosses were set up and maintained under a 12:12 hour
460 light:dark cycle at 18°C. Crosses were discarded after 5 days to maintain consistent
461 population density. Following eclosion, adult flies were collected and kept at 18°C for 2–3
462 days. $GAL80^{TS}$ driver activation was achieved by incubating the flies at 29°C for the
463 durations specified in each experiment. For experiments involving the GeneSwitch driver,
464 fly crosses were maintained at 25°C under a 12:12 hour light:dark cycle and discarded after
465 3 days. Adult progenies were collected and fed on food containing 200 μM RU486
466 (Mifepristone, Cayman Chemicals, 10006317), prepared by dissolving the compound in
467 95% ethanol before adding it to standard fly food. Flies were fed on RU486-containing food
468 for 7 days.

469 Esg^{ts} (*esg-Gal4, UAS-GFP, tub-GAL80^{TS}*), *Esg-LexA* and *LexAop-yki^{3SA}-GFP, Attp40 UAS-*
470 *Luciferase* are from the Perrimon lab stock collection.
471 The following strains were obtained from the Bloomington *Drosophila* Stock Center
472 (BL), Vienna Drosophila Resource Center (V) and flyORF (F): *UAS-Hnf4 RNAi* (BL# 29375),
473 *UAS-mElo RNAi* (BL# 44510), *UAS-yki^{3SA}* (BL#28817), *UAS-Pvf1-3xHA* (F002862), *UAS-*
474 *PvR[A]* (BL#58496), *UAS-Pvf1 RNAi* (V#102699), *UAS-PvR RNAi* (V#43459), *UAS-Luciferase*
475 *RNAi* (BL#31603), Oe^{ts} (*Desat1-Gal4, tubP-Gal80*) (BL# 65406), *UAS-LpR1 RNAi* (BL#
476 50737), *UAS-LpR2 RNAi* (BL# 54461).
477 *UAS-Hnf4* is a gift from Dr. Carl Thummel [31]; *UAS-TSC1, TSC2* is a gift from Dr.
478 Christen K Mirth [63] and UAS-PRAS40 was a gift from Dr. Aurelio Teleman [64], Btl^{TS} (*Btl-*
479 *Gal4, UAS-srcGFP*) and *QF6 >QUAS-mtdTomato* was a kind gift from Dr. Chrysoula Pitsouli
480 [26]. PromE^{GS}(*PromE-GeneSwitch-Gal4*) was a gift from Dr. Heinrich Jasper [65]. *UAS-*
481 *CG18609* and *mFas-Gal4* were gifts from Dr. Henry Chung [66, 67]. *UAS-PRAS40* is a gift
482 from Dr. Aurelio A Teleman [52].
483 Hnf4-127D01 was generated through CRISPR-mediated tagging of endogenous Hnf4
484 with 127D01-tag as described previously [32]. Briefly, we cloned the sequence 1 kb
485 upstream and 1 kb downstream of the stop codon into the donor vector pScarlessHD-C-
486 3x127D01-DsRed (Addgene#171578). A sgRNA plasmid pCFD3-Hnf4-sgRNA that target the
487 seed sequence (CCAGAGACTGGTTACTAGAAGAA) near the stop codon of Hnf4 was injected
488 into yw;nos-cas9/CyO embryos together with the donor plasmid. Positive transformants
489 with red eye fluorescent eyes were outcrossed and successful Kis were confirms by PCR (F:
490 GTACAACCGGAGCGAGGGTA; R: CAAAATGGTTCAAGGCATAACA) and sequencing.
491 Subsequently, 3xP3dsRed was excised using piggyBac transposase (BL#8285).
492
493 ***Untargeted lipidomic analysis***
494 Lipidomics and metabolomics of fly samples was performed following the Folch
495 method (Folch et al., 1957). 15 adult flies, or hemolymph from 200-300 adult flies were
496 used for lipidomics and metabolomics. Solid samples were homogenized in a 1 mL Dounce
497 homogenizer (TIGHT) on ice with 0.6 mL chloroform and 0.3 mL methanol (2:1 chloroform-

498 methanol mixture). Homogenized samples were transferred to a 15 mL glass tube with a
499 Teflon cap, and an additional 0.6 mL chloroform and 0.3 mL methanol were added to make
500 the final volume approximately 1.8 mL. Hemolymph was transferred to a 15 mL glass tube
501 containing 1.2 mL chloroform and 0.6 mL methanol (2:1 chloroform-methanol mixture).
502 Samples were vortexed briefly and incubated at room temperature on a rotator for 30–45
503 minutes. Following incubation, 0.2 volumes (0.36 mL) of HPLC-grade deionized water
504 (HPLC dH2O) were added. The mixture was vortexed three times, followed by
505 centrifugation at 1000 × g for 10 minutes at 4°.
506 The upper aqueous phase, containing polar metabolites, was carefully collected
507 using a glass pipette, while avoiding the middle phase. Metabolites were transferred to
508 microcentrifuge tubes, evaporated under vacuum using a SpeedVac rotary evaporator
509 overnight, and stored at -80°C. Polar metabolites were resuspended in 20 µL of HPLC-grade
510 water and then injected and analyzed using a hybrid 6500 QTRAP triple quadrupole mass
511 spectrometer (AB/SCIEX) connected to a Prominence UFLC HPLC system (Shimadzu). The
512 lower phase, containing non-polar lipids, was transferred to a clean 1.85 mL glass test tube
513 using a glass pipette. The phase was dried under nitrogen gas for approximately 30
514 minutes, and dried lipids were stored at -80°C to prevent oxidation. Non-polar lipids were
515 resuspended in 35 µL of HPLC-grade 50% methanol/50% isopropyl alcohol (IPA) and then
516 injected and analyzed using untargeted high-resolution LC-MS/MS on a Thermo QExactive
517 Plus Orbitrap mass spectrometer. LipidSearch version 4.2 (Thermo Scientific) was used to
518 identify lipid molecules, with the quantification of ion intensity by measuring the area size
519 of identified peaks.
520 The full names of the lipid species can be found in Supplementary Table 4. For
521 lipidomic quantification using whole fly bodies, the same number of flies was used for lipid
522 extraction. Lipid species were normalized to the total reads in each sample. For
523 hemolymph lipidomic analysis, lipid species were normalized to both the volume of
524 hemolymph extracted and the total reads in each sample.
525
526 ***RNA extraction Quantitative RT-PCR***

527 Adult female fly oenocytes were dissected in cold 1xPBS before RNA extraction. For
528 oenocyte dissection, the fat body was removed through liposuction and then oenocytes
529 were removed from the cuticle using a fine-tip glass needle. Tissue lysis, RNA extraction,
530 and cDNA synthesis were performed using Cells-to-CT Kit (Thermo Scientific, #44-029-53).
531 For female adult whole body mRNA extraction, four flies per biological replicate were
532 collected. Total RNA was extracted using Direct-zol RNA MicroPrep kit (Zymo Research,
533 #R2060). mRNA was extracted from HepG2 cells using Directo-zol RNA MicroPrep kit
534 (Zymo Research, #R2060). 30-50mg of mice livers were dissected and total RNA was
535 extracted using Qiagen RNeasy Mini kit (Qiagen #74104). All the cDNAs were synthesized
536 using the iScript cDNA synthesis kit (Bio-Rad, #1708896) in a 40ul reaction mixture using
537 1000ng total RNA. Quantitative real-time RT-PCR (RT-qPCR) assays were performed using
538 iQ SYBR Green Supermix (Bio-Rad, #1708880) on a CFX96 Real-Time PCR Detection
539 system (Bio-Rad). Two to four independent biological replicates were performed with two
540 technical replicates. The mRNA abundance of each gene was normalized to the expression
541 of *RpL32* or *αTub84B* for fly samples, Gapdh for mouse samples and ACTB for HepG2
542 samples. Primer sequences are listed in the Supplementary Table 5.
543
544 ***Fly imaging***
545 *Drosophila* ovaries were dissected in cold PBS. ovaries were imaged immediately in
546 cold PBS using a ZEISS Axiozoom V16 fluorescence microscope. Flies were anesthetized
547 on CO_2 pad and imaged using ZEISS Axiozoom V16 fluorescence microscope. The size of
548 the ovary and abdomen is measured using Fiji (version: 2.14.0/1.54f).
549
550 ***Oil Red O staining***
551 The method was as previously described [13]. Flies were dissected in PBS and fat
552 bodies were removed with liposuction. Specimens were fixed in 4% paraformaldehyde for
553 20 minutes. Specimens were rinsed twice with distilled water. Oil Red O (O0625-, Sigma-
554 Aldrich) was dissolved in isopropanol to make 0.1% Oil Red O stock. A working solution
555 was prepared by combining 3 mL of 0.1% Oil Red O in isopropanol with 2 mL of distilled

556 water. The solution was freshly prepared and filtered through a 0.2-μm syringe filter before
557 use. Specimens were incubated for 25 minutes in Oil Red O stain, rinsed briefly with PBS
558 and mounted in Vector Shield for imaging. Oil Red O images were taken using Olympus
559 VS200 Slide Scanner, equipped with color camera (2448x2048 pixels, 3.45μm).
560
561 ***Immunostaining and image analysis***
562 For immunostaining using the nanobodies, fly abdomens were dissected in PBS at
563 room temperature with fat bodies removed and fixed in 4% formaldehyde in PBS for 30
564 minutes. Specimens were washed three times in PBST (0.1% Triton-X-100), 5 minutes each.
565 The specimens were then incubated in 5% NGS (normal goat serum in PBST) for 1 hour.
566 Nb127D01-ALFA, 0.2mg/ml was used at a dilution of 1:500, incubating the samples for 1
567 hour and a half with mild shaking. Followed by 0.1% PBST washes, 5 minutes each wash.
568 AlexaFluor 594 anti-Alpaca (Jackson Immuno Research, 128-585-232) was diluted 1:400 in
569 PBS-TX + 5% NGS and incubate with the specimens at room temperature with mild shaking
570 for 1 hours. After washes and DAPI staining, tissues were mounted in Vectashield and
571 imaged with Olympus VS200 Slide Scanner or confocal microscope Zeiss Axio Observer Z1.
572 For regular immunostainings, fly tissues were dissected in PBS at room temperature.
573 Tissues were fixed in 4% paraformaldehyde in PBS for 30 minutes. Specimens were washed
574 three times in 0.1% PBST and incubated in 5% NDS solution for 1 hour. Tissues were then
575 incubated with primary antibodies diluted in PBST and blocking solution overnight at 4°.
576 Then the tissues were washed three times with PBST at room temperature. Secondary
577 antibodies were applied for 1 hour. Excess antibodies were washed in PBST, and tissues
578 were incubated with DAPI (Invitrogen, D1306) dilute in PBST for 5 minutes. Tissues were
579 then mounted in Vectashield (Vector Laboratories Inc, H-1000). The following primary
580 antibodies were used: rabbit-anti-pH3 (1:500, Cell Signaling, 9701), rabbit-anti-p4E-BP
581 (1:800, Cell Signaling, 2855S). Secondary antibodies against mouse, rabbit, chicken or
582 alpaca conjugated to Alexa Fluor 488 and 594 (Jackson Immuno Research) were used at
583 1:800 for anti-p-4EBP, 1:1000 for anti-pH3 and 1:400 for Nb127D01-ALFA.
584

585

586

587 ***Lifespan analysis***

588 For survival analysis, flies were collected within 24 hours post-eclosion (20 females
589 and 3 males per vial) and maintained on standard laboratory fly food at 18°C, with 60%
590 humidity, and a 12-hour light/dark cycle. After two days, mature and mated females were
591 transferred to 29°C to induce gene expression. To maintain vial cleanliness, flies were
592 transferred to fresh vials every two days, and the number of dead flies was recorded daily.

593

594 ***snRNAseq analysis***

595 Data and plots were generated from the Fly Cell Atlas, generated using the 10X
596 platform, "Stringent All" dataset. Other snRNAseq dataset was analyzed as described in
597 [35], where a resolution of 0.4 was chosen as the clustering parameter.
598 For the Seurat Module Score analysis, Seurat AddModuleScore function was used to
599 calculate the average expression of a group of genes in Very Long Chain Fatty Acid
600 Synthesis pathway in each cell (for details of the list, see Supplementary Table 6), then
601 subtracted by a randomly picked gene set expression.

602

603 ***Rapamycin feeding***

604 Rapamycin was dissolved in DMSO to make 2mM rapamycin stock. Rapamycin
605 stock was further diluted to 200μM in ethanol and evenly distributed on to food surface. A
606 small piece of Kimwipe was used to remove excess liquids on the food. DMSO dissolved in
607 ethanol was used as control. Flies were transferred to new food every two days. Flies were
608 fed for 6-7 days before dissection.

609

610 ***Dextran injection***

611 Using a fine glass needle, ~100nl of 50 mg/ml 10,000 MW TR-dextran (Thermo Fisher
612 Scientific, D-1817) diluted in water was injected in the abdomen of adult females. 6 hours
613 after injection, abdomen and thoraces were separated and whole abdomen were fixed in

4% paraformaldehyde for 30 minutes with mild shaking. After fixation, midguts were dissected and washed briefly with PBS and mounted in Vectashield. Midguts were imaged using a single point laser scanning confocal, Olympus IX83 to measure the trachea leakage. A Z-stack was taken, and maximum projections were used to generate final image for analysis.

Trachea imaging

Generating fly strains that incorporate both a trachea reporter and other genetic modifications is challenging. Therefore, the following method, as described in [26], was used to quantify the trachea. Flies were dissected in cold PBS, and intestines were carefully extracted to maintain their original structure. Tissues were then fixed in 4% paraformaldehyde for 20 minutes, mounted in Vectashield, and imaged within 3 days. Whole intestine images were captured using an Olympus VS200 Slide Scanner equipped with a color camera. Only the upper layer of the tissue, in contact with the coverslip, was analyzed.

Trachea analysis

To automate trachea measurement, we used the previously developed software AutoTube [68]. Only the topmost Z-stack, which provided the clearest image of the trachea, was analyzed. Images corresponding to the R2-R4 regions of the gut were cropped, avoiding areas with the major trunk of the trachea to prevent skewing the results. Images were thresholded on a white background and analyzed with AutoTube using the following settings:

- Input Color Channel: Green
- Intensity adjustment: Autocontrast
- Illumination correction: Illumination size set to 51
- Noise correction: BM3D
- Tube detection: Finer tubes with a tube size of 3
- Small regions removed: 0.01% of Ima

643 - Hole filling: Hole size set to 1
644 - Threshold type: MultiOtsu
645 - Short ramifications removed: Spur length set to 15
646 - Spatial branch merging: Spatial distance set to 10
647 The analysis provided results for "Number of Branches (μm)," "Total Tube Area (μm)," and
648 "Total Skeleton Length (μm)," which were normalized to the corresponding intestinal area
649 and were multiplied by an arbitrary number 1000000. Results from the R2-R4 regions were
650 averaged for each gut.
651
652 ***Animal Care and Tumor Induction***
653 *Kras*^{G12D}*/+;Lkb1*$^{f/f}$ mice, previously described [3, 69], were backcrossed to the FVB
654 strain. Male mice were maintained on a 12-hour light/dark cycle at an ambient temperature
655 of 22°C, with ad libitum access to rodent chow (PicoLab Rodent 5053; Lab Diet, 3.43
656 kcal/g) and drinking water. Tumors were induced in adult male and female mice (12 to 20
657 weeks old) via intranasal administration of 75 μL PBS containing 2.5×10^7 pfu of adenovirus
658 SMV-CRE (Ad5CMV-Cre) purchased from the University of Iowa Gene Transfer Vector Core
659 (Iowa City, IA). All animal experiments were conducted with the approval of the Institutional
660 Animal Care and Use Committee (IACUC) at Weill Cornell Medicine (WCM) under protocol
661 number 2013-0116.
662
663 ***Mice tissue collection***
664 Male mice were euthanized with CO_2, followed by blood collection via cardiac
665 puncture. Liver, gonadal adipose tissue, and skeletal muscles were dissected and flash-
666 frozen in liquid nitrogen and stored at -80°. The control mice were a mix of fasted and fed
667 mice. “Fasted” mice were fasted for 12 hours and “fed” mice were fasted for 12 hours and
668 then allowed free access to food for 4 hours before tissue collection.
669
670 ***VEGFA incubation***

HepG2 cells were cultured in HyClone Dulbecco's Modified Eagle Medium (DMEM) with high glucose (SH30022.01): with L-glutamine; without sodium pyruvate. Additional 50U penicillin/ml and 50ug streptomycin/ml were added. HepG2 cells were seeded at density of 5 x 10^5 in 12-well-plate (VWR, 29442-040), treated or not with 50ng/ml Recombinant Human VEGF 165 (PeproTech, 100-20-2UG) for 24 hours. Total cellular RNA was isolated using the Trizol reagent and extracted through Direct-zol RNA MicroPrep kit (Zymo Research, #R2060).

Acknowledgments

We thank Dr. John M. Asara at the Beth Israel Deaconess Medical Center for his help on lipidomic analysis. We thank the assistance provided by the Microscopy Resources on the North Quad (MicRoN) core and we thank Dr. Simon F. Norrelykke at the Image Analysis Collaboratory at Harvard Medical School for advice on AutoTube. We also thank Dr. Ah-Ram Kim, Dr. Sun Jin Moon at Harvard Medical School, Dr. Hua Bai at Iowa State University, Dr. Eileen White and Dr. Maria Gomez- Jenkins at Rutgers University for scientific discussion and insights. We thank Dr. Ju Xu at Chinese Academy of Sciences for the help generating Hnf4-127D01 fly strain. We also thank Christians Villalta for the help on fly dextran injection.

This article is subject to HHMI's Open Access to Publications policy. HHMI lab heads have previously granted a nonexclusive CC BY 4.0 license to the public and a sublicensable license to HHMI in their research articles. Pursuant to those licenses, the author-accepted manuscript of this article can be made freely available under a CC BY 4.0 license immediately upon publication.

Funding

This work is funded by NIH/NCI Grant #5P01CA120964-15 and is delivered as part of the CANCAN team supported by the Cancer Grand Challenges partnership funded by Cancer Research UK (CGCATF-2021/100022) and the National Cancer Institute (1 OT2 CA278685-01). N.P. is an investigator of the Howard Hughes Medical Institute.

700

701

702

703 **Author contributions**

704 Conceptualization: KH, TM, MG, NP; Methods, Data Acquisition, Resources,
705 Visualization and Imaging: KH, TM; Mice sample preparation: ED, JS; Data Acquisition: KW,
706 Bioinformatic Analysis: MH, YH; Independent replication of experiments at Harvard
707 Medical School: KH; Writing – original draft: KH, Writing – review, editing & revising: KH, TM,
708 NP.

709

710 **Figure 1: Oenocyte Hnf4 regulates wax ester synthesis and supports Yki-induced**
711 **tumor growth.**

712 (A-B) Heatmap of the normalized total ion intensity of major lipid classes identified in
713 whole bodies from control flies (*Esg-LexA*) or Yki flies (*Esg-LexA/LexAop-yki*^{S3A}*; PromE-*
714 *GAL4, Tub-GAL80*^{TS}/+), with four biological replicates per condition. Scaled colors are
715 presented as the values relative to the average of each row. (B) Untargeted lipidomic
716 profiling using LC-MS/MS of whole-body extracts revealed increased wax ester (WE) levels
717 in Yki flies. (C) WE level in oenocyte-specific knockdown of *Hnf4* using the RU486-inducible
718 *PromE*^{gs} driver (+RU) compared to controls (-RU). (D) WE level in control flies, Yki flies, and
719 *Hnf4* knockdown in oenocytes of Yki flies, N = 4 biological replicates. (E-F) Immunostaining
720 of Nb127D01 for nuclear-localized, endogenously tagged Hnf4 (Hnf4-127D01) in oenocytes
721 in controls and in Yki flies. DAPI staining marks nuclei, with dashed lines enclosing
722 oenocytes. N = 8 independent experiments. (G) Quantification of intestinal stem cell (ISC)
723 proliferation, as indicated by phospho-histone H3 (pH3+) cells in control. (H-I) Ovary sizes
724 and quantification. (J) Abdominal bloating. (K) UMAP from whole body (without head)
725 snRNAseq, *mElo* expression is enriched in adult oenocytes. (L) *mElo* expression in
726 oenocytes, normalized to housekeeping gene, in Yki flies and in Yki flies with *Hnf4*
727 knockdown. N = 2 biological replicates from 2 independent experiments. (M) Quantification
728 of pH3+ cell number, N =8 flies. (N) Oil Red O staining in oenocytes of *Hnf4* knockdown or

729 *mElo* knockdown. N = 8 flies. (O-P) Lifespan analysis showing that oenocyte-specific
730 knockdown of *Hnf4* (O) or *mElo* (P) in Yki flies, compared to only Yki or control flies, N = 40.
731 Scale bar shows 20μm. Data are presented as mean ± s.e.m. Statistical significance was
732 determined using Student's t-test or one-way ANOVA with appropriate post hoc tests, or
733 Log-rank (Mantel-Cox) test. *P < 0.05, **P < 0.01, ****P < 0.0001.
734
735 **Figure 1S: Hnf4 and mElo regulate metabolic and tumor-related phenotypes in Yki**
736 **flies.**
737 (A) Confirmation of *Hnf4* knockdown efficiency via qPCR, N = 2 biological replicates from 2
738 independent experiments. (B) Immunostaining of Nb127D01 for nuclear-localized,
739 endogenously tagged Hnf4 (Hnf4-127D01) in oenocytes with *Hnf4* knockdown or control
740 flies, with dashed lines enclosing oenocytes. (C-D) Oenocyte-specific *Hnf4* knockdown
741 reduces ovary size compared to control flies, quantification in (D), n = 9 - 15. (E) Wet weight
742 measurement of fly whole body, N = 3 biological replicates. (F) Expression of VLCFA
743 biosynthesis and β-oxidation genes in control and Yki flies. (G-H) *mElo* expression
744 measured by qPCR in oenocyte specific *Hnf4* knockdown or *Hnf4* overexpression, N = 2
745 biological replicates from 2 independent experiments. (I) Confirmation of *mElo* knockdown
746 efficiency via qPCR. (J-K) Ovary size in oenocyte *mElo* knockdown flies compared to
747 control, quantification in (K). (L) Ovary size measurement in control and Yki flies, N = 8-10
748 flies. (M) Lifespan analysis in Yki-expressing flies upon oenocyte-specific *mElo* knockdown
749 in male flies. Data represent mean ± s.e.m.; significance assessed using appropriate
750 statistical tests.
751
752 **Figure 2: TORC1 regulates Hnf4 activity and lipid metabolism in oenocytes.**
753 (A) snRNAseq analysis showing *Hnf4* expression in fat body, muscle and oenocytes upon
754 overexpression of *TSC1,2* in oenocytes. (B-C) Immunostaining of Hnf4-127D01 in
755 oenocytes when *TSC1,2* is overexpressed in oenocytes compared to control. DAPI marks
756 nuclei, with dashed lines enclosing oenocytes, quantification of Hnf4-127D01 signal
757 intensity in the nucleus, N = 8-10 flies. (D) ModuleScore from snRNAseq analysis visualizes

758 VLCFA synthesis gene expression across muscle, fat body and oenocytes, in control and
759 upon oenocyte *TSC1,2* overexpression. (E) ORO staining indicates steatosis in oenocytes
760 induced by *TSC1,2* overexpression, and in *TSC1,2* with *Hnf4* overexpression, N = 8. (F-G)
761 Expression of Hnf4 targets *mElo* and *FASN2* in *TSC1,2* overexpression and in *TSC1,2* with
762 *Hnf4* overexpression. N = 2 biological replicates from 2 independent experiments. (H)
763 Whole body WE level in ISC Yki flies and Yki with oenocyte *TSC1,2* overexpression. (I-J) P-
764 4EBP immunostaining indicates TORC1 activity in oenocytes of Yki flies, quantification of P-
765 4EBP intensity is shown on the right (J), N = 8-10 flies. (K) *mElo* expression in whole body
766 mRNA extracts in Yki flies and Yki flies with *TSC1,2* overexpression in oenocytes, N = 6
767 biological samples. (L) Quantification of pH3+ cell number, N = 8 – 10 flies. (M) Ovary size
768 measurements are rescued by *TSC1,2* overexpression in Yki flies, N = 15-30 flies.
769
770 **Figure 2S: The role of oenocyte TORC1 in regulating lifespan, steatosis and Yki wasting**
771 **phenotype.**
772 (A) Sensitivity to dry starvation in flies overexpressing *TSC1,2* in oenocytes compared to
773 controls. Adult oenocyte specific driver (*mFas-Gal4*) was used [66]. (B-C) ORO staining
774 indicates steatosis in oenocytes with *PRAS40* overexpression, or in rapamycin treatment.
775 (D) Host bloating quantification in fly abdomen in Yki flies and in Yki flies with *TSC1,2*
776 overexpression, compared to control. Dashed lines enclose oenocytes in all
777 immunostaining images. Data represent mean ± s.e.m.; statistical significance determined
778 using Student's t-test or ANOVA as appropriate.
779
780 **Figure 3: ISCs secreted Pvf1 activates Hnf4 through PvR signaling in oenocytes and**
781 **affects tumor associated phenotypes.**
782 (A-B) Immunostaining of Hnf4-127D01 nuclear localization in oenocytes upon *Pvf1*
783 overexpression in ISCs (*Esg>Pvf1*). Dashed lines enclose oenocytes. N = 10 biological
784 replicates. (C) *mElo* expression in oenocytes following ISC-specific *Pvf1* overexpression. N
785 = 4 biological replicates from 2 independent experiments. (D-F) Immunostaining and qPCR
786 analysis reveal Hnf4-127D01 nuclear localization and *mElo* expression in oenocytes

787 overexpressing active *PvR*. (G-H) Immunostaining of Hnf4-127D01 in oenocytes of Yki flies
788 (*Esg>yki^{3SA};Luc-i*) and flies with knockdown of *Pvf1* in Yki flies (*Esg> yki^{3SA};Pvf1-i*). N = 10
789 biological replicates. (I) *mElo* expression in oenocytes of *Esg>yki^{3SA};Pvf1-i* flies, N = 4
790 biological replicates from 2 independent experiments. (J-K) Inhibition of *Pvf1* in the gut
791 affects bloating and ovary size in Yki flies, n = 15-20 flies. (L) ISC mitosis (pH3+ cells) in
792 *Esg>yki^{3SA};Pvf1-i* flies, n = 8-10 biological replicates. (M) Yki-induced *mElo* expression. Dual
793 LexA and Gal4 systems to express *yki^{3SA}* in ISCs and mediate knockdown of *PvR* in
794 oenocytes (*Esg-LexA> yki^{3SA}; PromE>PvR-i*). N = 2 biological replicates from 2 independent
795 experiments. (N-P) *PvR* knockdown in oenocytes and its effect on tumor-associated
796 bloating (N), ovary wasting (O), and pH3+ cell number (P), N = 10-20 flies. (Q) Lifespan
797 extension in Yki flies with oenocyte-specific *PvR* knockdown, N = 40 flies. Dashed lines
798 enclose oenocytes in all immunostaining images. Data are presented as mean ± s.e.m.;
799 statistical significance was assessed using Student's t-test or ANOVA.
800
801 **Figure 3S: Expression of *Pvf1* in fly whole body and oenocytes in Yki flies.**
802 UMAP from whole body (without head) snRNAseq, shows *Pvf1* expression level, oenocyte
803 cluster is marked as "oe". (B) snRNAseq analysis on oenocyte *Pvf1* expression in control
804 (*Esg>+)* and Yki flies (*Esg>yki^{3SA}*) at 5 days. (C) snRNAseq analysis of oenocyte *Pvf1*
805 expression at 8 days of *yki^{3SA}* induction.
806
807 **Figure 4: Circulating lipids target trachea but not ISCs to promote tracheal growth.**
808 Untargeted lipidomic analysis of fly hemolymph showing lipid species in control, Yki flies,
809 and Yki flies with oenocyte-specific *Hnf4* knockdown (*Esg>yki^{3SA};PromE>Hnf4-i*). N = 4
810 biological replicates. (B-C) Levels of very-long-acylcarnitines (AcCa 24:1 and AcCa 24:2) in
811 Yki flies with or without *Hnf4* knockdown in oenocytes. (D-E) Levels of circulating
812 phospholipids, including PC 36:4 PE 32:5, across experimental conditions. (F-G) Levels of
813 circulating TG 18:3_16:0_16:1 and TG 18:2_16:0_18:0 in the fly hemolymph. (H) Counts of
814 pH3+ cells in the midgut of flies with oenocyte-specific *TSC1*,2 overexpression or *Hnf4*
815 knockdown or overexpression. N = 8-20 flies. (I-K) Number of tracheal branches, tube area,

816 and skeleton length in Yki flies with ISC-specific knockdown of *LpR1* and *LpR2*. (L) pH3+
817 cell counts in ISCs of Yki flies with ISC-specific knockdown of *LpR1* and *LpR2*. (M-O) Effects
818 of trachea-specific knockdown of *LpR1* and *LpR2* using the *Btl-Gal4* driver on trachea
819 parameters, including number of branches, tube area, and skeleton length, compared to
820 control flies (*Btl>ctrl*). N = 8-12 flies. Dashed lines enclose oenocytes in all relevant images.
821 Data are presented as mean ± s.e.m.; statistical analysis was performed using Student's t-
822 test or ANOVA as appropriate.
823
824 **Figure 4S: Effects of ISC-specific *LpR1* and *LpR2* knockdown on tracheal morphology**
825 **and ISC proliferation.**
826 (A-C) Trachea parameters, including number of branches, tube area, and skeleton length,
827 in flies with ISC-specific knockdown of *LpR1* and *LpR2* using *Esg* driver, compared to
828 control (*Esg>ctrl*). N = 7-11 flies. (D) Counts of pH3+ cells in the midgut of flies with ISC-
829 specific knockdown of *LpR1* and *LpR2*, compared to controls. (E) Counts of pH3+ cells in
830 the midgut of flies with trachea-specific knockdown of *LpR1* and *LpR2*, compared to
831 controls. N=8-10 flies. Data are presented as mean ± s.e.m.; statistical analysis was
832 performed using Student's t-test or ANOVA as appropriate.
833
834 **Figure 5: Hnf4-mElo axis regulates tracheogenesis in the midgut.**
835 (A-B) Whole-body wax ester (WE) levels in flies with oenocyte-specific *Hnf4* knockdown
836 (*PromE^{gs}>Hnf4-i*), *mElo* knockdown (*PromE^{gs}>mElo-i*), or *TSC1,2* overexpression
837 (*PromE^{gs}>TSC1,2*). N = 3-4 biological replicates (C) Transepithelial barrier function of the
838 trachea on the midgut, assessed using red dextran injection, in flies with oenocyte-specific
839 *Hnf4* knockdown. N = 8 flies. (D-G) Trachea morphology on the midgut (R2-R4), including
840 branch number and skeleton length normalized to gut surface area, in flies with *Hnf4*
841 knockdown in oenocytes. N = 8 flies. (H-J) Branch number, tube area, and skeleton length
842 of the midgut trachea in flies with oenocyte-specific *mElo* knockdown. N = 6-8 flies (K-P)
843 Number of branches, tracheal tube area and skeleton length of the midgut in flies
844 overexpressing *Hnf4* or *mElo* in oenocytes (*PromE^{gs}>Hnf4* or *PromE^{gs}>mElo*). N = 8-15 flies.

845

846 **Figure 5S: Effect of oenocyte Hnf4 on ovary trachea.**

847 (A-D) Tracheal branch number, tube area and total skeleton length of the ovary in flies with
848 *Hnf4* knockdown in oenocytes. N = 8 flies. (E-G) Comparison of gut trachea morphology in
849 wild type flies (*PromE*^{gs}>+) with and without RU feeding. N = 12 flies. Dashed lines enclose
850 oenocytes in all relevant images. Data are presented as mean ± s.e.m.; statistical analysis
851 was performed using Student's t-test or ANOVA as appropriate.

852

853 **Figure 6: Hnf4-mElo axis in oenocytes mediates lipid metabolism and tracheogenesis**
854 **induced by Yki tumors.**

855 (A-C) Number of tracheal branches, total tube area, and total tube length in the midgut of
856 Yki flies with oenocyte-specific *TSC1,2* overexpression, *Hnf4* knockdown, or *mElo*
857 knockdown. N = 9-17 flies. (D-F) Tracheal morphology measurements, including number of
858 branches and skeleton length, in flies with ISC-specific knockdown of *Pvf1* combined with
859 *yki* overexpression (*Esg>yki*^{3SA}*;Pvf1-i*). N = 9-11 flies. Dashed lines enclose oenocytes in all
860 relevant images. Data are presented as mean ± s.e.m.; statistical analysis was performed
861 using Student's t-test or ANOVA as appropriate.

862

863 **Figure 6S: Hnf4-mElo axis in oenocytes mediates lipid metabolism and tracheogenesis**
864 **induced by Yki tumors.**

865 (A-D) Tracheal morphology parameters, including number of branches, total tube area,
866 total tube length, and skeleton length, in Yki midgut (*Esg>yki*), compared to wild-type
867 controls (*Esg>ctrl*). N = 16-17. (E) Whole-body wax ester (WE) levels in Yki flies with
868 oenocyte-specific *Hnf4* knockdown (Esg-LexA>LexAop-yki^{3SA}; *PromE>Hnf4-i*) or *TSC1,2*
869 overexpression (Esg-LexA>LexAop-yki^{3SA}; *PromE>TSC1,2*), measured to investigate the role
870 of lipid metabolism in trachea growth. N = 4 biological replicates.

871

872 **Figure 7: Regulation of hepatocyte lipid metabolism by pro-angiogenic factors in**
873 **tumor models.**

874 (A-E) Relative expression levels of *ELOVL* fatty acid elongase 1–7 in HepG2 cells incubated
875 with vascular endothelial growth factor A (VEGF-A) for 24 hours, compared to controls. N =
876 4 biological replicates, from 2 independent experiments. (F-G) Relative expression levels of
877 *Hnf4a* and *Elovl7* in liver samples from *KrasG12D/+;Lkb1f/f* (KL) tumor-bearing mice
878 compared to control mice. N = 4 biological replicates, from 2 independent experiments. (H)
879 Schematic representation of the proposed mechanism, depicting tumor-secreted
880 PDGF/VEGF-like factors activating the mTOR-Hnf4 axis in hepatocyte-like oenocytes to
881 promote lipid synthesis, which are then transported to trachea. Dashed lines indicate
882 hepatocyte regions or cells analyzed. Data are presented as mean ± s.e.m.; statistical
883 analysis was performed using Student's t-test.
884

885 **References**

886 1. Anderson, N.M. and M.C. Simon, *The tumor microenvironment*. Curr Biol, 2020.
887 **30**(16): p. R921-r925.
888 2. Chen, X., et al., *Neural Circuitries between the Brain and Peripheral Solid Tumors*.
889 Cancer Res, 2024. **84**(21): p. 3509-3521.
890 3. Goncalves, M.D., et al., *Fenofibrate prevents skeletal muscle loss in mice with lung*
891 *cancer*. Proceedings of the National Academy of Sciences, 2018. **115**(4): p. E743-
892 E752.
893 4. Schutz, Y., *Protein turnover, ureagenesis and gluconeogenesis*. Int J Vitam Nutr Res,
894 2011. **81**(2-3): p. 101-7.
895 5. Lee, J.S., et al., *Urea Cycle Dysregulation Generates Clinically Relevant Genomic*
896 *and Biochemical Signatures*. Cell, 2018. **174**(6): p. 1559-1570 e22.
897 6. Al-Zoughbi, W. and G. Hoefler, *Tumor Macroenvironment: An Update*. Pathobiology,
898 2020. **87**(2): p. 58-60.
899 7. Jin, H.-R., et al., *Lipid metabolic reprogramming in tumor microenvironment: from*
900 *mechanisms to therapeutics*. Journal of Hematology & Oncology, 2023. **16**(1): p.
901 103.
902 8. Wang, H., et al., *CD36-mediated metabolic adaptation supports regulatory T cell*
903 *survival and function in tumors*. Nat Immunol, 2020. **21**(3): p. 298-308.
904 9. Wu, L., et al., *RIPK3 Orchestrates Fatty Acid Metabolism in Tumor-Associated*
905 *Macrophages and Hepatocarcinogenesis*. Cancer Immunol Res, 2020. **8**(5): p. 710-
906 721.
907 10. Veglia, F., et al., *Fatty acid transport protein 2 reprograms neutrophils in cancer*.
908 Nature, 2019. **569**(7754): p. 73-78.
909 11. Bilder, D., et al., *Tumour-host interactions through the lens of Drosophila*. Nat Rev
910 Cancer, 2021. **21**(11): p. 687-700.

911 12. Droujinine, I.A. and N. Perrimon, *Interorgan Communication Pathways in Physiology:*
912 *Focus on Drosophila*. Annu Rev Genet, 2016. **50**: p. 539-570.
913 13. Gutierrez, E., et al., *Specialized hepatocyte-like cells regulate Drosophila lipid*
914 *metabolism*. Nature, 2007. **445**(7125): p. 275-80.
915 14. Chatterjee, D., et al., *Control of metabolic adaptation to fasting by dILP6-induced*
916 *insulin signaling in Drosophila oenocytes*. Proc Natl Acad Sci U S A, 2014. **111**(50):
917 p. 17959-64.
918 15. Billeter, J.C., et al., *Specialized cells tag sexual and species identity in Drosophila*
919 *melanogaster*. Nature, 2009. **461**(7266): p. 987-91.
920 16. Ferveur, J.F., et al., *Genetic feminization of pheromones and its behavioral*
921 *consequences in Drosophila males*. Science, 1997. **276**(5318): p. 1555-8.
922 17. Blomquist, G.J., A.J. Chu, and S. Remaley, *Biosynthesis of wax in the honeybee, Apis*
923 *mellifera L*. Insect Biochemistry, 1980. **10**(3): p. 313-321.
924 18. Qiu, Y., et al., *An insect-specific P450 oxidative decarbonylase for cuticular*
925 *hydrocarbon biosynthesis*. Proc Natl Acad Sci U S A, 2012. **109**(37): p. 14858-63.
926 19. Reed, J.R., et al., *Unusual mechanism of hydrocarbon formation in the housefly:*
927 *cytochrome P450 converts aldehyde to the sex pheromone component (Z)-9-*
928 *tricosene and CO2*. Proceedings of the National Academy of Sciences, 1994. **91**(21):
929 p. 10000-10004.
930 20. Wicker-Thomas, C., et al., *Flexible origin of hydrocarbon/pheromone precursors in*
931 *Drosophila melanogaster*. J Lipid Res, 2015. **56**(11): p. 2094-101.
932 21. Wang, Z., et al., *Evolution of a fatty acyl-CoA elongase underlies desert adaptation in*
933 *Drosophila*. Sci Adv, 2023. **9**(35): p. eadg0328.
934 22. Labeur, C., R. Dallerac, and C. Wicker-Thomas, *Involvement of desat1 gene in the*
935 *control of Drosophila melanogaster pheromone biosynthesis*. Genetica, 2002.
936 **114**(3): p. 269-74.
937 23. Storelli, G., et al., *Drosophila HNF4 Directs a Switch in Lipid Metabolism that*
938 *Supports the Transition to Adulthood*. Dev Cell, 2019. **48**(2): p. 200-214 e6.
939 24. Ghabrial, A., et al., *Branching morphogenesis of the Drosophila tracheal system*.
940 Annu Rev Cell Dev Biol, 2003. **19**: p. 623-47.
941 25. Li, Z., et al., *Trachea-derived dpp controls adult midgut homeostasis in Drosophila*.
942 Dev Cell, 2013. **24**(2): p. 133-43.
943 26. Tamamouna, V., et al., *Remodelling of oxygen-transporting tracheoles drives*
944 *intestinal regeneration and tumorigenesis in Drosophila*. Nat Cell Biol, 2021. **23**(5):
945 p. 497-510.
946 27. Perochon, J., et al., *Dynamic adult tracheal plasticity drives stem cell adaptation to*
947 *changes in intestinal homeostasis in Drosophila*. Nat Cell Biol, 2021. **23**(5): p. 485-
948 496.
949 28. Kwon, Y., et al., *Systemic organ wasting induced by localized expression of the*
950 *secreted insulin/IGF antagonist ImpL2*. Dev Cell, 2015. **33**(1): p. 36-46.
951 29. Kwon, Y., et al., *Systemic Organ Wasting Induced by Localized Expression of the*
952 *Secreted Insulin/IGF Antagonist ImpL2*. Developmental Cell, 2015. **33**(1): p. 36-46.
953 30. Patel, S., D.R. Nelson, and A.G. Gibbs, *Chemical and physical analyses of wax ester*
954 *properties*. J Insect Sci, 2001. **1**: p. 4.

31. Palanker, L., et al., *Drosophila HNF4 Regulates Lipid Mobilization and β-Oxidation*. Cell Metabolism, 2009. **9**(3): p. 228-239.
32. Xu, J., et al., *Protein visualization and manipulation in Drosophila through the use of epitope tags recognized by nanobodies*. eLife, 2022. **11**: p. e74326.
33. Bradley, M.E., et al., *Potent and Efficacious Inhibition of CXCR2 Signaling by Biparatopic Nanobodies Combining Two Distinct Modes of Action*. Molecular Pharmacology, 2015. **87**(2): p. 251-262.
34. Palanker, L., et al., *Drosophila HNF4 regulates lipid mobilization and beta-oxidation*. Cell Metab, 2009. **9**(3): p. 228-39.
35. Ghosh, A.C., et al., *Drosophila PDGF/VEGF signaling from muscles to hepatocyte-like cells protects against obesity*. eLife, 2020. **9**: p. e56969.
36. Zhang, Y., et al., *Rheb is a direct target of the tuberous sclerosis tumour suppressor proteins*. Nature Cell Biology, 2003. **5**(6): p. 578-581.
37. Sopko, R., et al., *A systems-level interrogation identifies regulators of Drosophila blood cell number and survival*. PLoS Genet, 2015. **11**(3): p. e1005056.
38. Tran, T.A., et al., *Platelet-derived growth factor/vascular endothelial growth factor receptor inactivation by sunitinib results in Tsc1/Tsc2-dependent inhibition of TORC1*. Mol Cell Biol, 2013. **33**(19): p. 3762-79.
39. Song, W., et al., *Tumor-Derived Ligands Trigger Tumor Growth and Host Wasting via Differential MEK Activation*. Dev Cell, 2019. **48**(2): p. 277-286 e6.
40. Otsubo, C., et al., *Long-chain Acylcarnitines Reduce Lung Function by Inhibiting Pulmonary Surfactant**. Journal of Biological Chemistry, 2015. **290**(39): p. 23897-23904.
41. Wolrab, D., et al., *Oncolipidomics: Mass spectrometric quantitation of lipids in cancer research*. TrAC Trends in Analytical Chemistry, 2019. **120**: p. 115480.
42. Cruciani, G., et al., *Diagnostic application of lipidomics fingerprints to bladder carcinoma*. Translational Cancer Research, 2017. **6**(6): p. 1197-1206.
43. Palm, W., et al., *Lipoproteins in Drosophila melanogaster--assembly, function, and influence on tissue lipid composition*. PLoS Genet, 2012. **8**(7): p. e1002828.
44. Khaliullina, H., et al., *Patched regulates Smoothened trafficking using lipoprotein-derived lipids*. Development, 2009. **136**(24): p. 4111-21.
45. Locke, M., *Pore canals and related structures in insect cuticle*. J Biophys Biochem Cytol, 1961. **10**(4): p. 589-618.
46. Moussian, B., *Recent advances in understanding mechanisms of insect cuticle differentiation*. Insect Biochem Mol Biol, 2010. **40**(5): p. 363-75.
47. Moussian, B., et al., *Cuticle differentiation during Drosophila embryogenesis*. Arthropod Struct Dev, 2006. **35**(3): p. 137-52.
48. Jaspers, M.H., et al., *The fatty acyl-CoA reductase Waterproof mediates airway clearance in Drosophila*. Dev Biol, 2014. **385**(1): p. 23-31.
49. Ding, G., et al., *Coordination of tumor growth and host wasting by tumor-derived Upd3*. Cell Rep, 2021. **36**(7): p. 109553.
50. Xu, J., et al., *Mechanistic characterization of a Drosophila model of paraneoplastic nephrotic syndrome*. Nature Communications, 2024. **15**(1): p. 1241.

51. Duvel, K., et al., *Activation of a metabolic gene regulatory network downstream of mTOR complex 1*. Mol Cell, 2010. **39**(2): p. 171-83.
52. Tiebe, M., et al., *REPTOR and REPTOR-BP Regulate Organismal Metabolism and Transcription Downstream of TORC1*. Dev Cell, 2015. **33**(3): p. 272-84.
53. Jiang, H., et al., *Cytokine/Jak/Stat signaling mediates regeneration and homeostasis in the Drosophila midgut*. Cell, 2009. **137**(7): p. 1343-55.
54. Buchon, N., et al., *Drosophila intestinal response to bacterial infection: activation of host defense and stem cell proliferation*. Cell Host Microbe, 2009. **5**(2): p. 200-11.
55. Apidianakis, Y., et al., *Synergy between bacterial infection and genetic predisposition in intestinal dysplasia*. Proc Natl Acad Sci U S A, 2009. **106**(49): p. 20883-8.
56. Amcheslavsky, A., et al., *Enteroendocrine Cells Support Intestinal Stem-Cell-Mediated Homeostasis in Drosophila*. Cell Reports, 2014. **9**(1): p. 32-39.
57. Lin, G., N. Xu, and R. Xi, *Paracrine Wingless signalling controls self-renewal of Drosophila intestinal stem cells*. Nature, 2008. **455**(7216): p. 1119-1123.
58. Schönfeld, P. and G. Reiser, *Brain Lipotoxicity of Phytanic Acid and Very Long-chain Fatty Acids. Harmful Cellular/Mitochondrial Activities in Refsum Disease and X-Linked Adrenoleukodystrophy.* Aging Dis, 2016. **7**(2): p. 136-49.
59. Baarine, M., et al., *Evidence of oxidative stress in very long chain fatty acid--treated oligodendrocytes and potentialization of ROS production using RNA interference-directed knockdown of ABCD1 and ACOX1 peroxisomal proteins*. Neuroscience, 2012. **213**: p. 1-18.
60. Zarrouk, A., et al., *Induction of mitochondrial changes associated with oxidative stress on very long chain fatty acids (C22:0, C24:0, or C26:0)-treated human neuronal cells (SK-NB-E)*. Oxid Med Cell Longev, 2012. **2012**: p. 623257.
61. Tamura, K., et al., *Novel lipogenic enzyme ELOVL7 is involved in prostate cancer growth through saturated long-chain fatty acid metabolism*. Cancer Res, 2009. **69**(20): p. 8133-40.
62. Karlsson, M., et al., *A single–cell type transcriptomics map of human tissues*. Science Advances, 2021. **7**(31): p. eabh2169.
63. Koyama, T. and C.K. Mirth, *Growth-Blocking Peptides As Nutrition-Sensitive Signals for Insulin Secretion and Body Size Regulation*. PLoS Biol, 2016. **14**(2): p. e1002392.
64. Pallares-Cartes, C., G. Cakan-Akdogan, and Aurelio A. Teleman, *Tissue-Specific Coupling between Insulin/IGF and TORC1 Signaling via PRAS40 in Drosophila*. Developmental Cell, 2012. **22**(1): p. 172-182.
65. Chatterjee, D., et al., *Control of metabolic adaptation to fasting by dILP6-induced insulin signaling in Drosophila oenocytes*. Proceedings of the National Academy of Sciences, 2014. **111**(50): p. 17959-17964.
66. Chung, H., et al., *A Single Gene Affects Both Ecological Divergence and Mate Choice in Drosophila*. Science, 2014. **343**(6175): p. 1148-1151.
67. Wang, Z., et al., *Evolution of a fatty acyl–CoA elongase underlies desert adaptation in Drosophila*. Science Advances, 2023. **9**(35): p. eadg0328.

68. Montoya-Zegarra, J.A., et al., *AutoTube: a novel software for the automated morphometric analysis of vascular networks in tissues*. Angiogenesis, 2019. **22**(2): p. 223-236.
69. Ji, H., et al., *LKB1 modulates lung cancer differentiation and metastasis*. Nature, 2007. **448**(7155): p. 807-810.

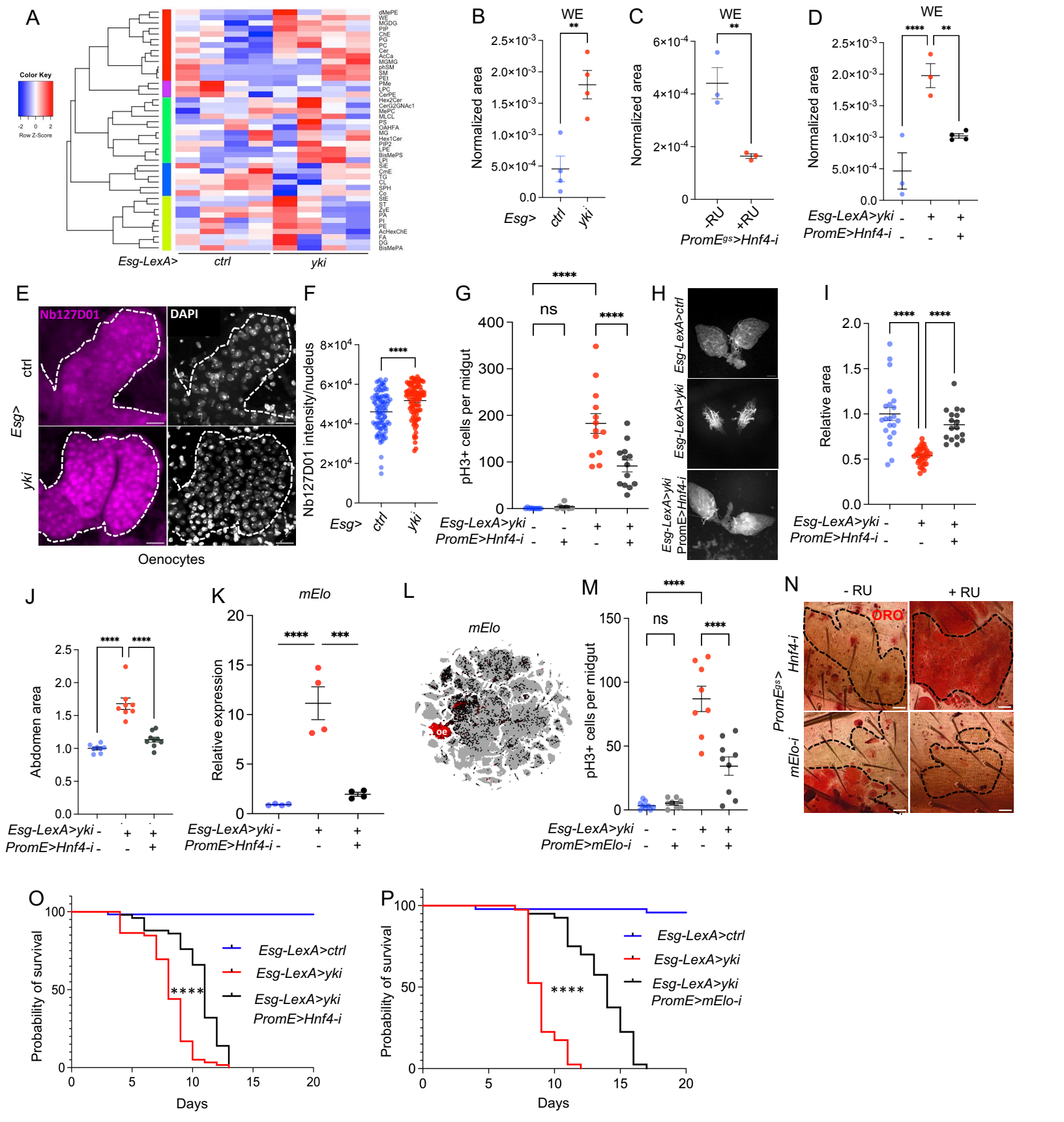
A
Color Key
Row Z-Score
dMePE
WE
MGDG
PIP
ChE
PG
PC
Cer
AcCa
MGMG
phSM
SM
PEt
PMe
LPC
CerPE
Hex2Cer
CerG2GNAc1
MePC
MLCL
PS
OAHFA
MG
Hex1Cer
PIP2
LPE
BisMePS
LPI
SiE
CmE
TG
CL
SPH
Co
StE
ST
ZyE
PA
PI
PE
AcHexChE
FA
DG
BisMePA
Esg-LexA>
ctrl
yki
B
WE
Normalized area
Esg>
ctrl
yki
C
WE
Normalized area
-RU
+RU
PromEgs>Hnf4-i
D
WE
Normalized area
Esg-LexA>yki
PromE>Hnf4-i
E
Nb127D01
DAPI
ctrl
Esg>
yki
Oenocytes
F
Nb127D01 intensity/nucleus
Esg>
ctrl
yki
G
ns
pH3+ cells per midgut
Esg-LexA>yki
PromE>Hnf4-i
H
Esg-LexA>ctrl
Esg-LexA>yki
Esg-LexA>yki PromE>Hnf4-i
I
Relative area
Esg-LexA>yki
PromE>Hnf4-i
J
Abdomen area
Esg-LexA>yki
PromE>Hnf4-i
K
mElo
Relative expression
Esg-LexA>yki
PromE>Hnf4-i
L
mElo
oe
M
ns
pH3+ cells per midgut
Esg-LexA>yki
PromE>mElo-i
N
- RU
+ RU
ORO
PromEgs>
Hnf4-i
mElo-i
O
Probability of survival
Days
Esg-LexA>ctrl
Esg-LexA>yki
Esg-LexA>yki PromE>Hnf4-i
P
Probability of survival
Days
Esg-LexA>ctrl
Esg-LexA>yki
Esg-LexA>yki PromE>mElo-i

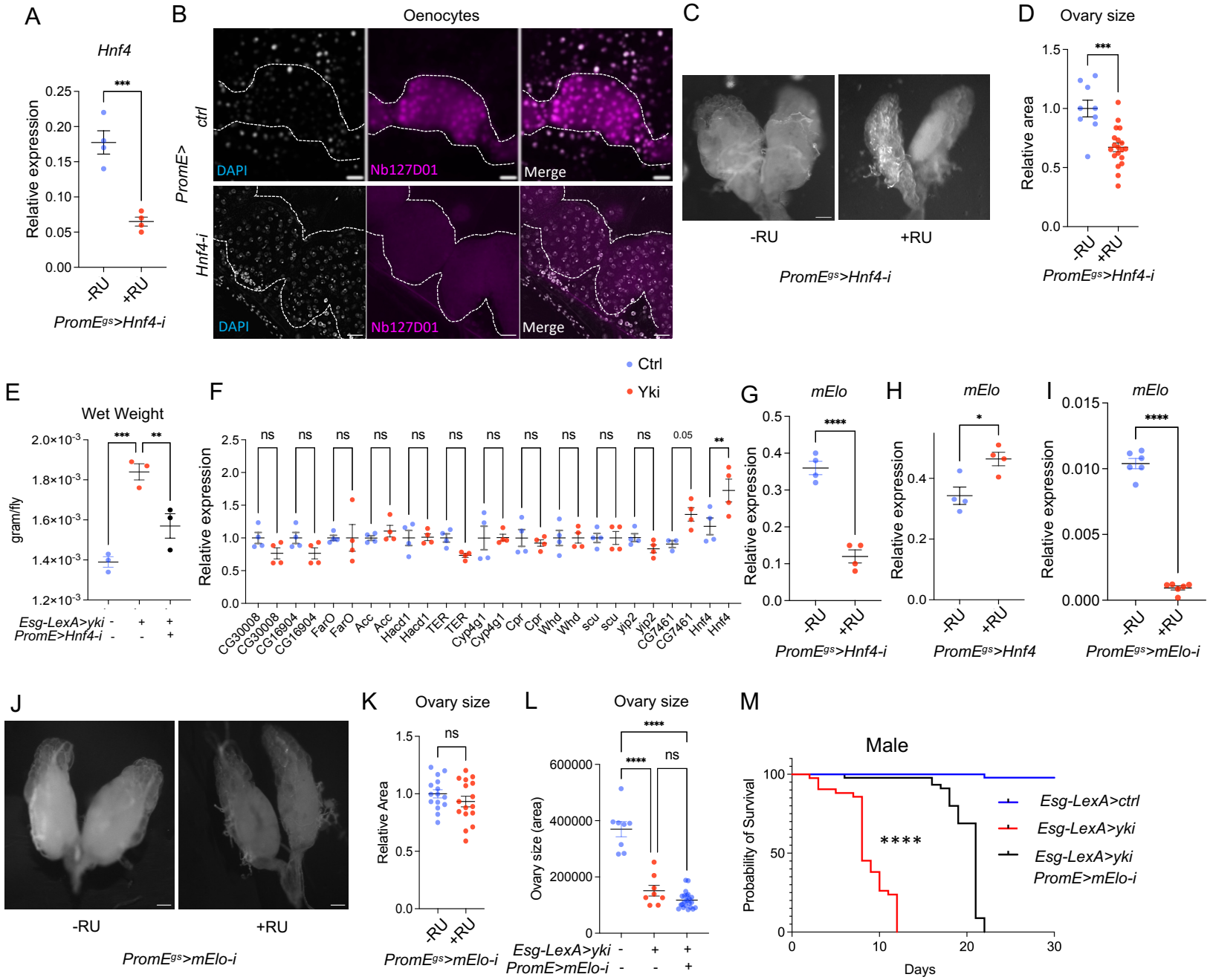
A
Hnf4
Relative expression
0.25
0.20
0.15
0.10
0.05
0.00
***
-RU
+RU
PromE^gs>Hnf4-i
B
Oenocytes
PromE>
ctrl
Hnf4-i
DAPI
Nb127D01
Merge
C
-RU
+RU
PromE^gs>Hnf4-i
D
Ovary size
Relative area
1.5
1.0
0.5
0.0
***
-RU
+RU
PromE^gs>Hnf4-i
E
Wet Weight
gram/fly
2.0×10^-3
1.8×10^-3
1.6×10^-3
1.4×10^-3
1.2×10^-3
***
**
Esg-LexA>yki - + +
PromE>Hnf4-i - - +
F
Ctrl
Yki
Relative expression
ns
0.05
**
CG30008
CG30008
CG16904
CG16904
FarO
FarO
Acc
Acc
Hacd1
Hacd1
TER
TER
Cyp4g1
Cyp4g1
Cpr
Cpr
Whd
Whd
scu
scu
yip2
yip2
CG7461
CG7461
Hnf4
Hnf4
G
mEIo
Relative expression
****
-RU
+RU
PromE^gs>Hnf4-i
H
mEIo
Relative expression
*
-RU
+RU
PromE^gs>Hnf4
I
mEIo
Relative expression
0.015
0.010
0.005
0.000
****
-RU
+RU
PromE^gs>mEIo-i
J
-RU
+RU
PromE^gs>mEIo-i
K
Ovary size
Relative Area
ns
-RU
+RU
PromE^gs>mEIo-i
L
Ovary size
Ovary size (area)
600000
400000
200000
0
****
****
ns
Esg-LexA>yki - + +
PromE>mEIo-i - - +
M
Male
Probability of Survival
100
50
0
****
Esg-LexA>ctrl
Esg-LexA>yki
Esg-LexA>yki
PromE>mEIo-i
0
10
20
30
Days

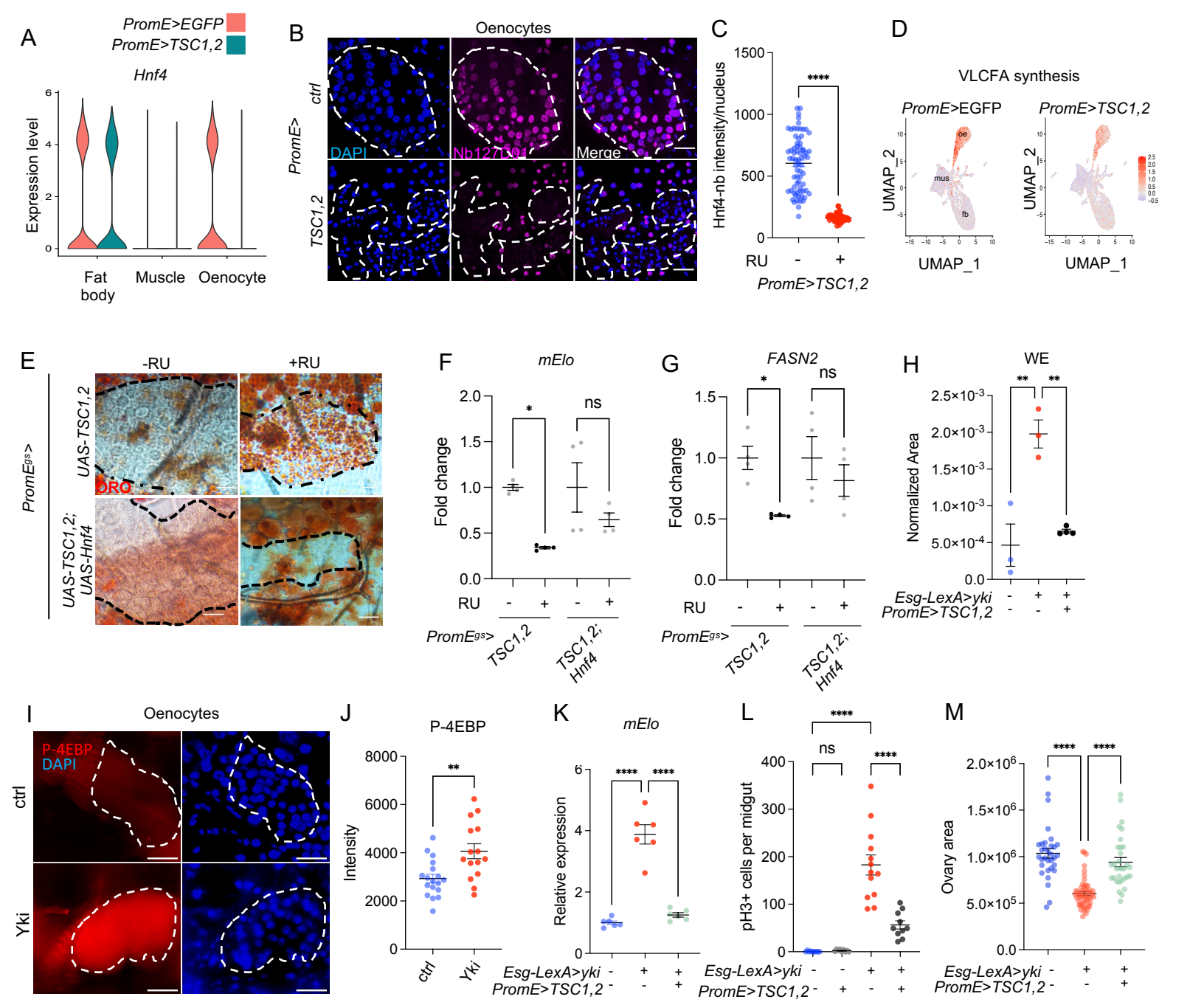
A
PromE>EGFP
PromE>TSC1,2
Hnf4
Expression level
Fat body
Muscle
Oenocyte
B
Oenocytes
ctrl
PromE>
TSC1,2
DAPI
Nb127D01
Merge
C
Hnf4-nb intensity/nucleus
****
RU
PromE>TSC1,2
D
VLCFA synthesis
PromE>EGFP
PromE>TSC1,2
UMAP_2
UMAP_1
oe
mus
fb
E
-RU
+RU
PromEgs>
UAS-TSC1,2
UAS-TSC1,2; UAS-Hnf4
ORO
F
mEIo
Fold change
*
ns
RU
PromEgs>
TSC1,2
TSC1,2; Hnf4
G
FASN2
Fold change
*
ns
RU
PromEgs>
TSC1,2
TSC1,2; Hnf4
H
WE
Normalized Area
**
**
Esg-LexA>yki
PromE>TSC1,2
I
Oenocytes
P-4EBP
DAPI
ctrl
Yki
J
P-4EBP
Intensity
**
ctrl
Yki
K
mEIo
Relative expression
****
****
Esg-LexA>yki
PromE>TSC1,2
L
pH3+ cells per midgut
ns
****
****
Esg-LexA>yki
PromE>TSC1,2
M
Ovary area
****
****
Esg-LexA>yki
PromE>TSC1,2

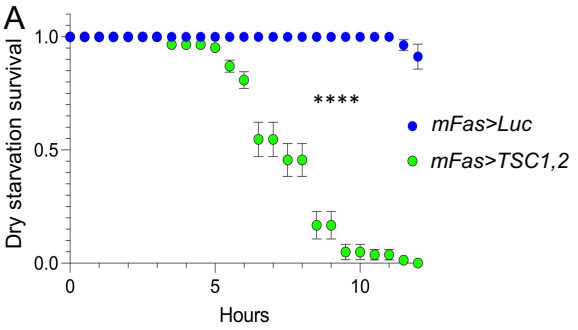
A
Dry starvation survival
1.0
0.5
0.0
0
5
10
Hours
****
mFas>Luc
mFas>TSC1,2

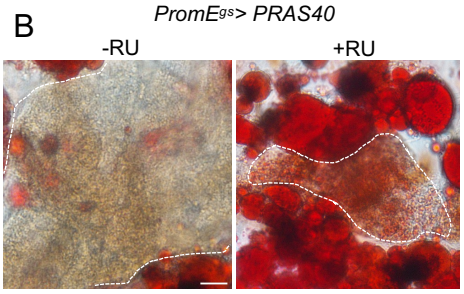
B
PromEgs> PRAS40
-RU
+RU

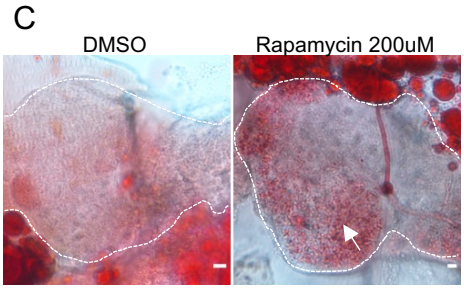
C
DMSO
Rapamycin 200uM

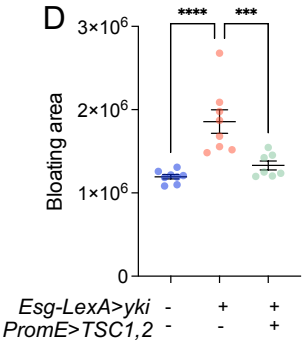
D
Bloating area
3×10^6
2×10^6
1×10^6
0
****
***
Esg-LexA>yki - + +
PromE>TSC1,2 - - +

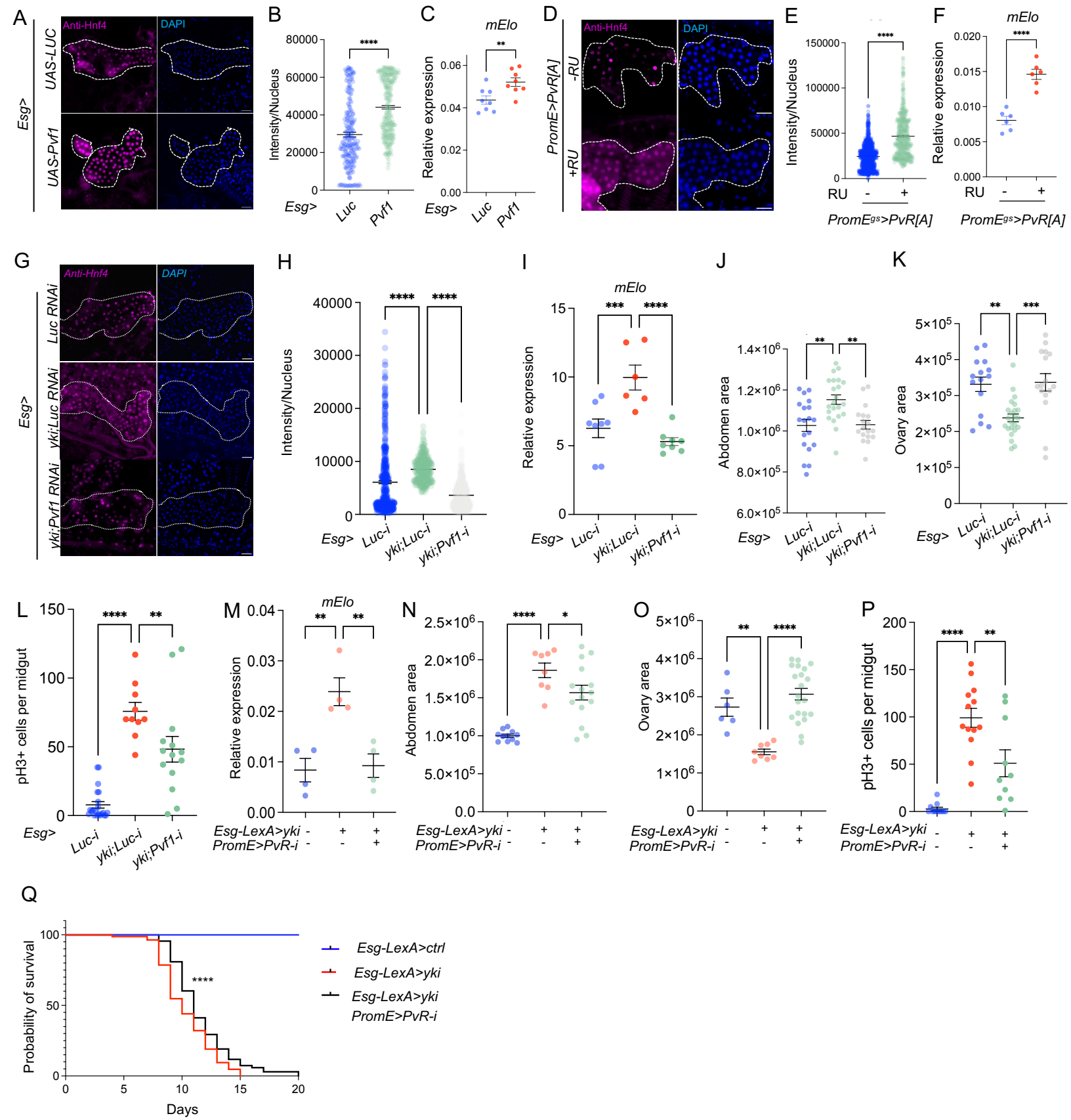
A
Anti-Hnf4
DAPI
Esg>
UAS-LUC
UAS-Pvf1
B
Intensity/Nucleus
Esg>
Luc
Pvf1
C
mElo
Relative expression
D
PromE>PvR[A]
-RU
+RU
E
Intensity/Nucleus
RU
PromEgs>PvR[A]
F
mElo
Relative expression
G
Luc RNAi
yki;Luc RNAi
yki;Pvf1 RNAi
H
Intensity/Nucleus
Luc-i
yki;Luc-i
yki;Pvf1-i
I
mElo
Relative expression
J
Abdomen area
K
Ovary area
L
pH3+ cells per midgut
M
mElo
Relative expression
Esg-LexA>yki
PromE>PvR-i
N
Abdomen area
O
Ovary area
P
pH3+ cells per midgut
Q
Probability of survival
Days
Esg-LexA>ctrl
Esg-LexA>yki
Esg-LexA>yki
PromE>PvR-i

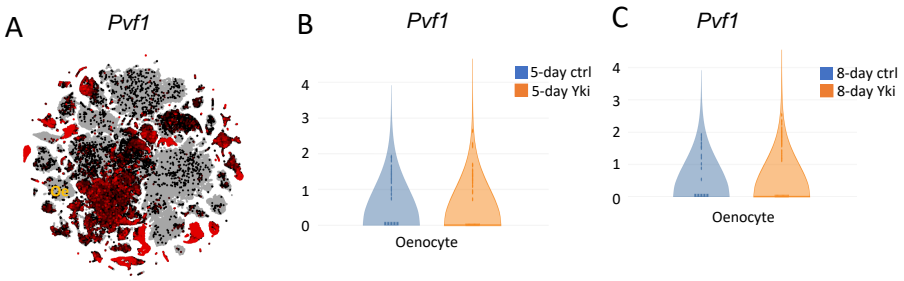
A
Pvf1
B
Pvf1
5-day ctrl
5-day Yki
4
3
2
1
0
Oenocyte
C
Pvf1
8-day ctrl
8-day Yki
4
3
2
1
0
Oenocyte

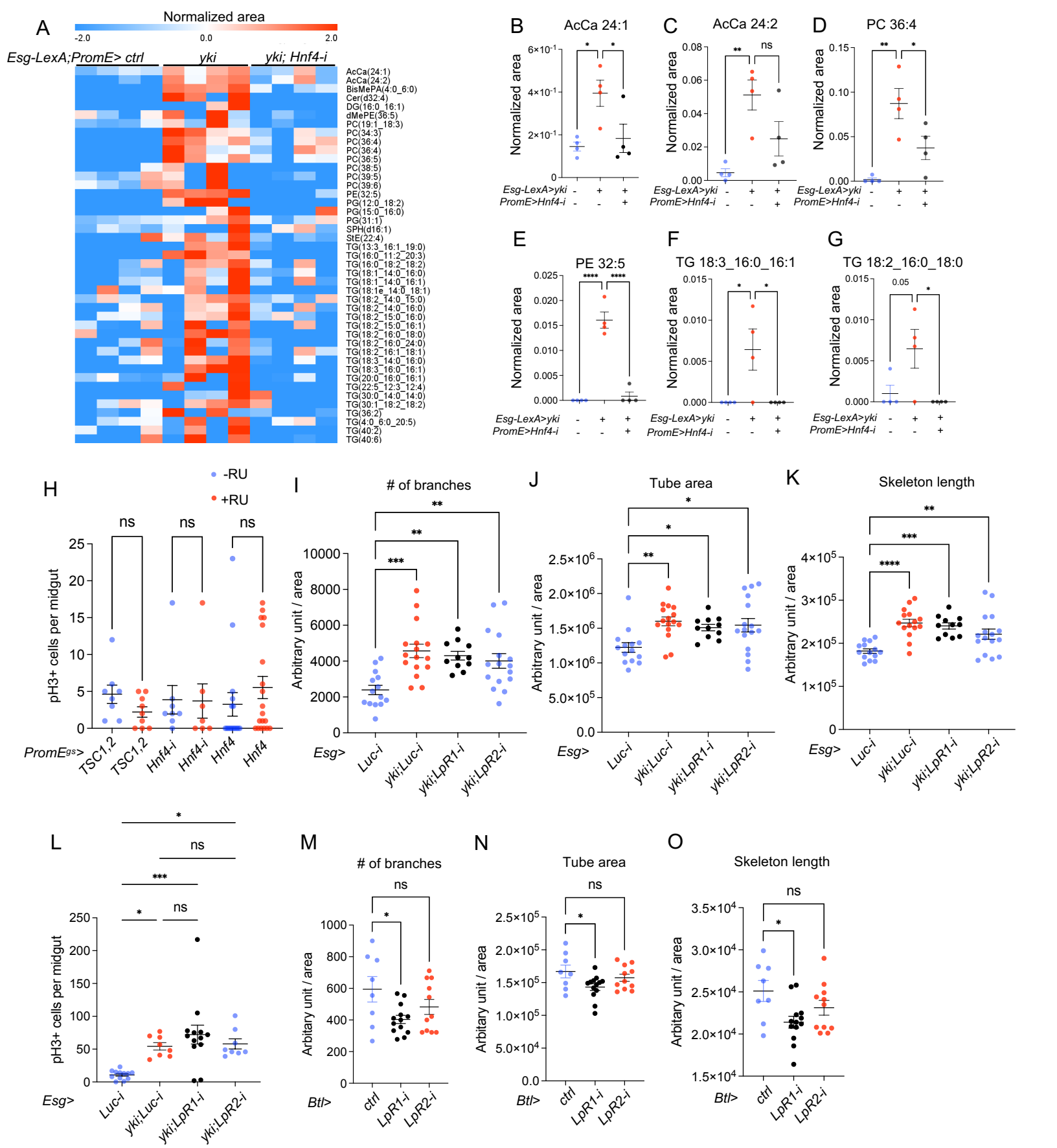
A
Normalized area
-2.0
0.0
2.0
Esg-LexA;PromE> ctrl
yki
yki; Hnf4-i
AcCa(24:1)
AcCa(24:2)
BisMePA(4:0_6:0)
Cer(d32:4)
DG(16:0_16:1)
dMePE(36:5)
PC(19:1_18:3)
PC(34:3)
PC(36:4)
PC(36:4)
PC(36:5)
PC(38:5)
PC(39:5)
PC(39:6)
PE(32:5)
PG(12:0_18:2)
PG(15:0_16:0)
PG(31:1)
SPH(d16:1)
StE(22:4)
TG(13:3_16:1_19:0)
TG(16:0_11:2_20:3)
TG(16:0_18:2_18:2)
TG(18:1_14:0_16:0)
TG(18:1_14:0_16:1)
TG(18:1e_14:0_18:1)
TG(18:2_14:0_15:0)
TG(18:2_14:0_16:0)
TG(18:2_15:0_16:0)
TG(18:2_15:0_16:1)
TG(18:2_16:0_18:0)
TG(18:2_16:0_24:0)
TG(18:2_16:1_18:1)
TG(18:3_14:0_16:0)
TG(18:3_16:0_16:1)
TG(20:0_16:0_16:1)
TG(22:5_12:3_12:4)
TG(30:0_14:0_14:0)
TG(30:1_18:2_18:2)
TG(36:2)
TG(4:0_6:0_20:5)
TG(40:2)
TG(40:6)
B
AcCa 24:1
C
AcCa 24:2
D
PC 36:4
E
PE 32:5
F
TG 18:3_16:0_16:1
G
TG 18:2_16:0_18:0
Normalized area
Esg-LexA>yki
PromE>Hnf4-i
H
-RU
+RU
ns
pH3+ cells per midgut
PromEgs>
TSC1,2
Hnf4-i
Hnf4
I
# of branches
Arbitrary unit / area
Esg>
Luc-i
yki;Luc-i
yki;LpR1-i
yki;LpR2-i
J
Tube area
K
Skeleton length
L
M
N
O
Arbitary unit / area
Btl>
ctrl
LpR1-i
LpR2-i

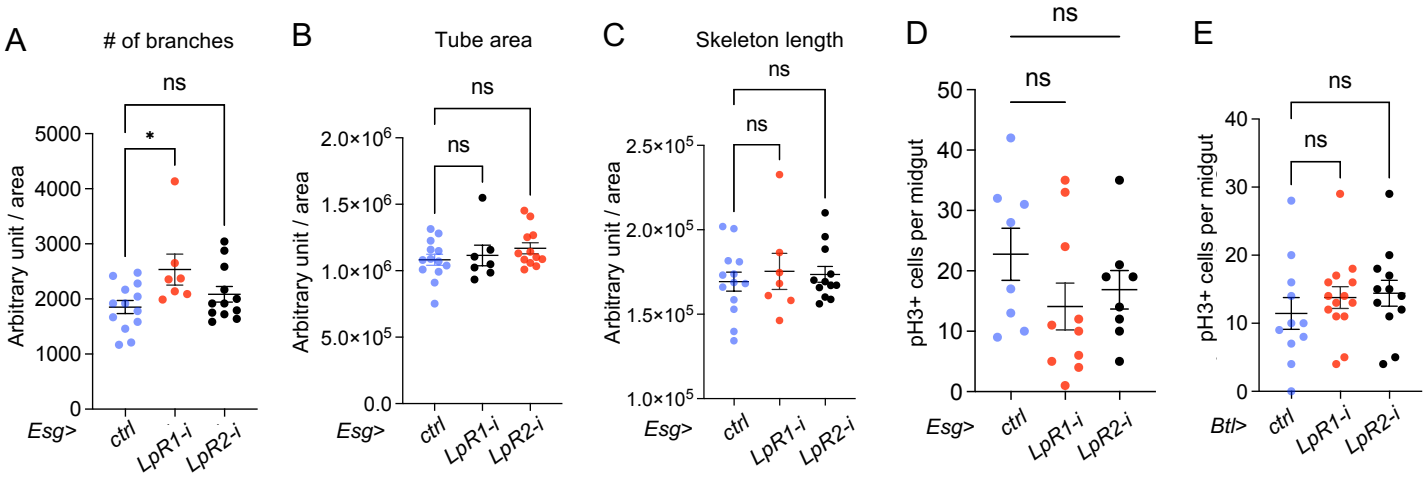
A
# of branches
ns
*
Arbitrary unit / area
5000
4000
3000
2000
1000
0
Esg>
ctrl
LpR1-i
LpR2-i
B
Tube area
ns
ns
Arbitrary unit / area
2.0×10^6
1.5×10^6
1.0×10^6
5.0×10^5
0.0
Esg>
ctrl
LpR1-i
LpR2-i
C
Skeleton length
ns
ns
Arbitrary unit / area
2.5×10^5
2.0×10^5
1.5×10^5
1.0×10^5
Esg>
ctrl
LpR1-i
LpR2-i
D
ns
ns
pH3+ cells per midgut
50
40
30
20
10
0
Esg>
ctrl
LpR1-i
LpR2-i
E
ns
ns
pH3+ cells per midgut
40
30
20
10
0
Btl>
ctrl
LpR1-i
LpR2-i

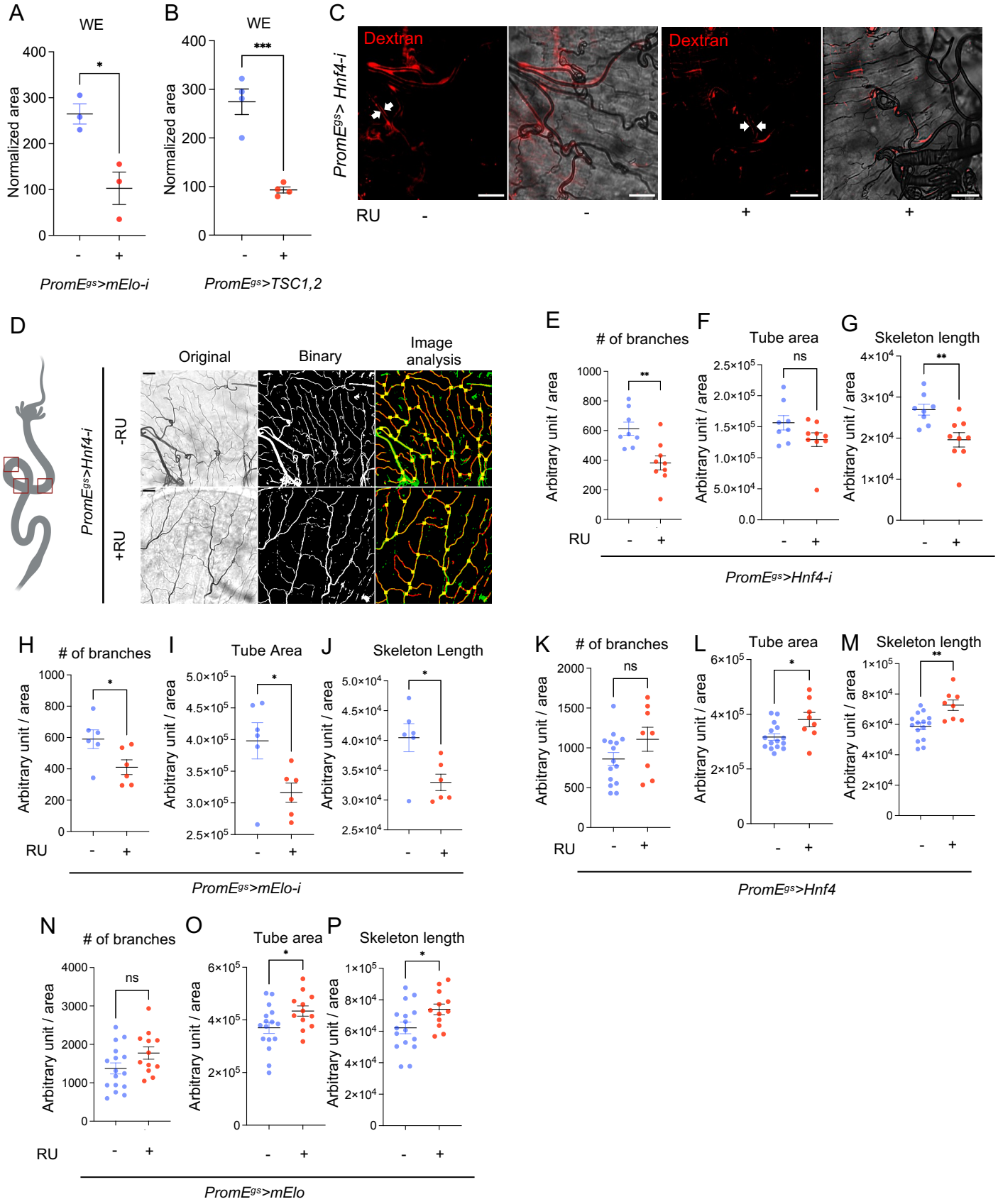
A
WE
Normalized area
400
300
200
100
0
*
-
+
PromEgs>mElo-i
B
WE
Normalized area
400
300
200
100
0
***
-
+
PromEgs>TSC1,2
C
PromEgs> Hnf4-i
Dextran
Dextran
RU
-
-
+
+
D
PromEgs>Hnf4-i
-RU
+RU
Original
Binary
Image analysis
E
# of branches
Arbitrary unit / area
1000
800
600
400
200
0
**
RU
-
+
F
Tube area
Arbitrary unit / area
2.5×10^5
2.0×10^5
1.5×10^5
1.0×10^5
5.0×10^4
0.0
ns
-
+
G
Skeleton length
Arbitrary unit / area
4×10^4
3×10^4
2×10^4
1×10^4
0
**
-
+
PromEgs>Hnf4-i
H
# of branches
Arbitrary unit / area
1000
800
600
400
200
0
*
RU
-
+
I
Tube Area
Arbitrary unit / area
5.0×10^5
4.5×10^5
4.0×10^5
3.5×10^5
3.0×10^5
2.5×10^5
*
-
+
J
Skeleton Length
Arbitrary unit / area
5.0×10^4
4.5×10^4
4.0×10^4
3.5×10^4
3.0×10^4
2.5×10^4
*
-
+
PromEgs>mElo-i
K
# of branches
Arbitrary unit / area
2000
1500
1000
500
0
ns
RU
-
+
L
Tube area
Arbitrary unit / area
6×10^5
4×10^5
2×10^5
0
*
-
+
M
Skeleton length
Arbitrary unit / area
1×10^5
8×10^4
6×10^4
4×10^4
2×10^4
0
**
-
+
PromEgs>Hnf4
N
# of branches
Arbitrary unit / area
4000
3000
2000
1000
0
ns
RU
-
+
O
Tube area
Arbitrary unit / area
6×10^5
4×10^5
2×10^5
0
*
-
+
P
Skeleton length
Arbitrary unit / area
1×10^5
8×10^4
6×10^4
4×10^4
2×10^4
0
*
-
+
PromEgs>mElo

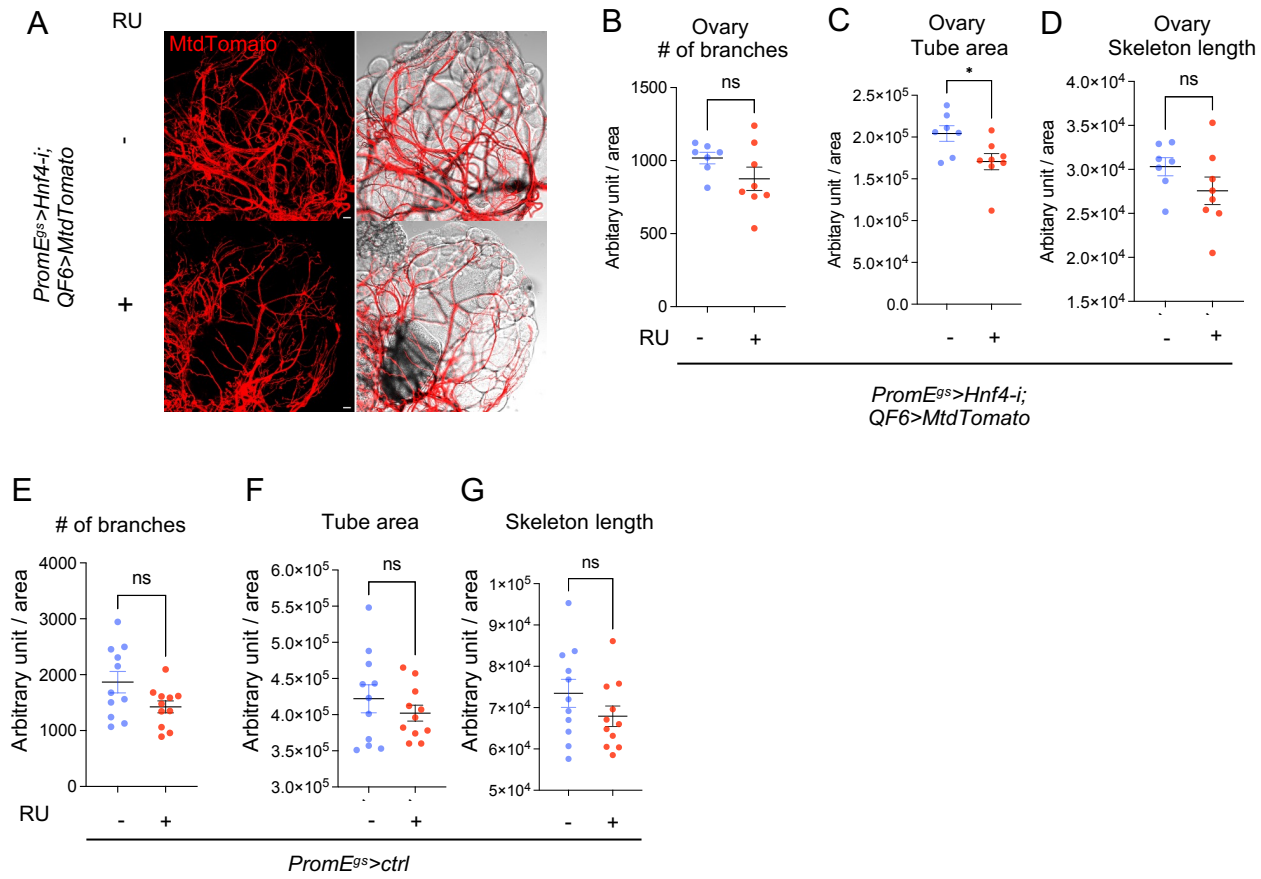
A
RU
MtdTomato
-
+
PromE^gs>Hnf4-i; QF6>MtdTomato
B
Ovary
# of branches
ns
Arbitary unit / area
1500
1000
500
0
RU
-
+
C
Ovary
Tube area
*
Arbitary unit / area
2.5×10^5
2.0×10^5
1.5×10^5
1.0×10^5
5.0×10^4
0.0
D
Ovary
Skeleton length
ns
Arbitary unit / area
4.0×10^4
3.5×10^4
3.0×10^4
2.5×10^4
2.0×10^4
1.5×10^4
PromE^gs>Hnf4-i; QF6>MtdTomato
E
# of branches
ns
Arbitrary unit / area
4000
3000
2000
1000
0
RU
F
Tube area
ns
Arbitrary unit / area
6.0×10^5
5.5×10^5
5.0×10^5
4.5×10^5
4.0×10^5
3.5×10^5
3.0×10^5
G
Skeleton length
ns
Arbitrary unit / area
1×10^5
9×10^4
8×10^4
7×10^4
6×10^4
5×10^4
PromE^gs>ctrl

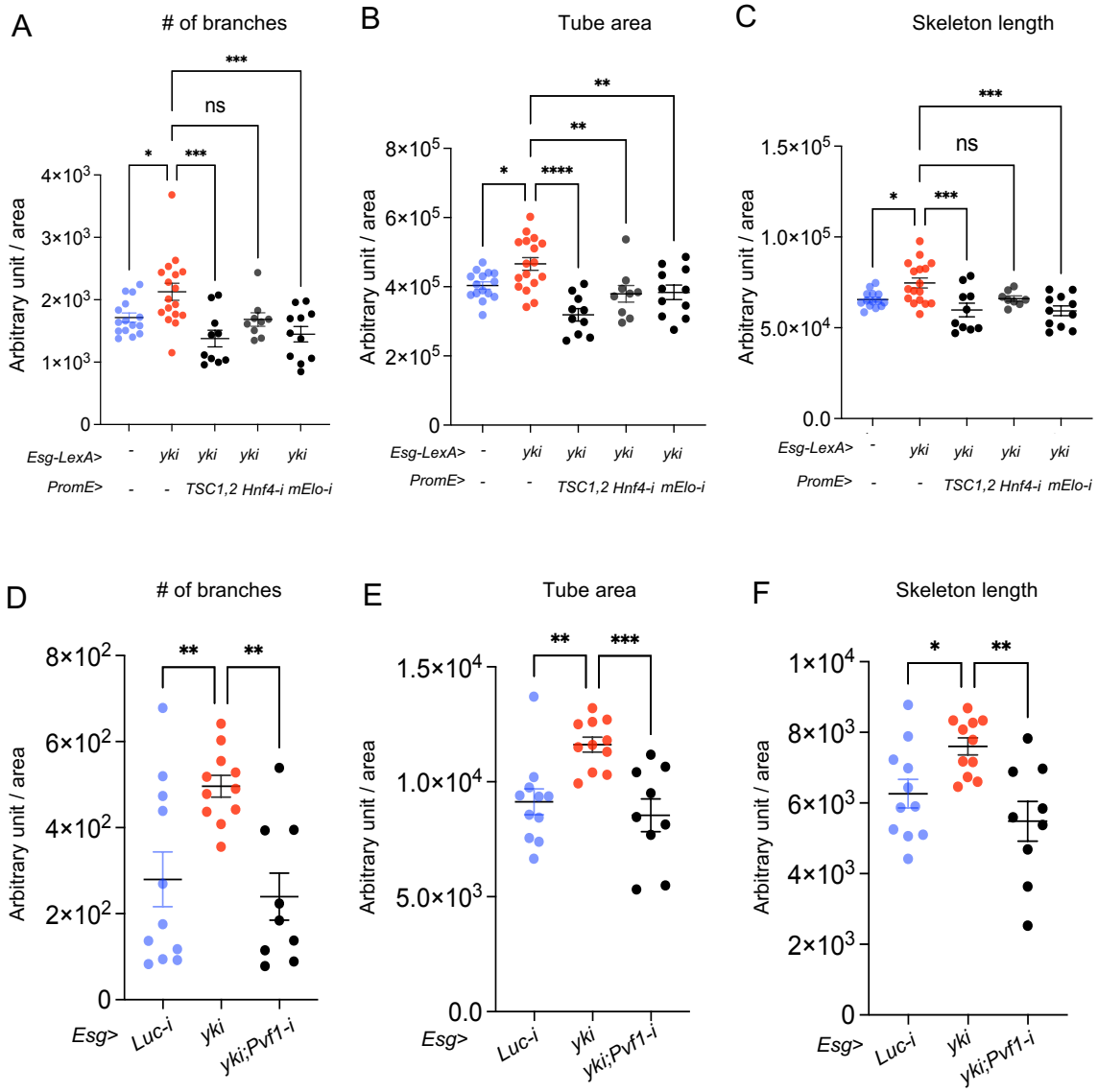
A
# of branches
Arbitrary unit / area
4×10^3
3×10^3
2×10^3
1×10^3
0
*
***
ns
***
Esg-LexA> - yki yki yki yki
PromE> - - TSC1,2 Hnf4-i mElo-i
B
Tube area
Arbitrary unit / area
8×10^5
6×10^5
4×10^5
2×10^5
0
*
****
**
**
Esg-LexA> - yki yki yki yki
PromE> - - TSC1,2 Hnf4-i mElo-i
C
Skeleton length
Arbitrary unit / area
1.5×10^5
1.0×10^5
5.0×10^4
0.0
*
***
ns
***
Esg-LexA> - yki yki yki yki
PromE> - - TSC1,2 Hnf4-i mElo-i
D
# of branches
Arbitrary unit / area
8×10^2
6×10^2
4×10^2
2×10^2
0
**
**
Esg> Luc-i yki yki;Pvf1-i
E
Tube area
Arbitrary unit / area
1.5×10^4
1.0×10^4
5.0×10^3
0.0
**
***
Esg> Luc-i yki yki;Pvf1-i
F
Skeleton length
Arbitrary unit / area
1×10^4
8×10^3
6×10^3
4×10^3
2×10^3
0
*
**
Esg> Luc-i yki yki;Pvf1-i

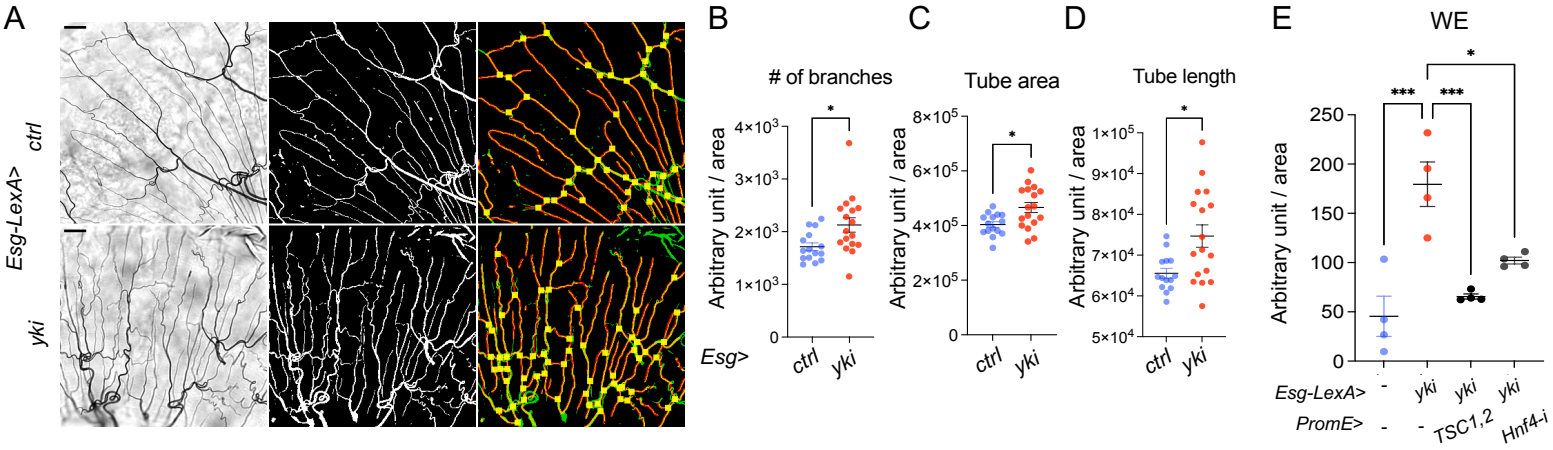
A
Esg-LexA>
ctrl
yki
B
# of branches
Arbitrary unit / area
4×10^3
3×10^3
2×10^3
1×10^3
0
*
Esg>
ctrl
yki
C
Tube area
Arbitrary unit / area
8×10^5
6×10^5
4×10^5
2×10^5
0
*
ctrl
yki
D
Tube length
Arbitrary unit / area
1×10^5
9×10^4
8×10^4
7×10^4
6×10^4
5×10^4
*
ctrl
yki
E
WE
Arbitrary unit / area
250
200
150
100
50
0
***
***
*
Esg-LexA>
PromE>
yki
yki
yki
TSC1,2
Hnf4-i

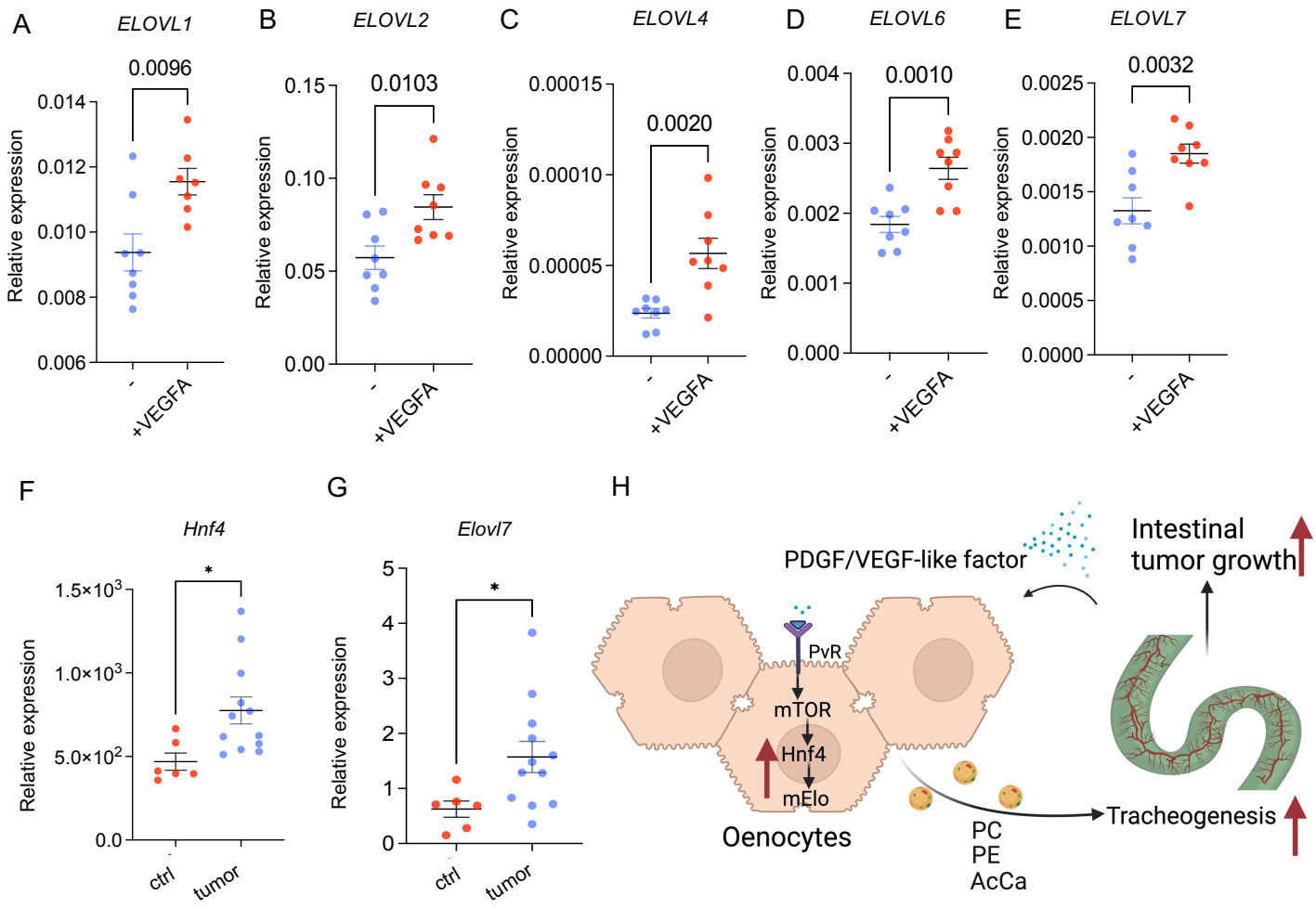
A
ELOVL1
0.0096
Relative expression
0.014
0.012
0.010
0.008
0.006
-
+VEGFA
B
ELOVL2
0.0103
0.15
0.10
0.05
0.00
C
ELOVL4
0.0020
0.00015
0.00010
0.00005
0.00000
D
ELOVL6
0.0010
0.004
0.003
0.002
0.001
0.000
E
ELOVL7
0.0032
0.0025
0.0020
0.0015
0.0010
0.0005
0.0000
F
Hnf4
*
1.5×10^3
1.0×10^3
5.0×10^2
0.0
ctrl
tumor
G
Elovl7
*
5
4
3
2
1
0
H
PDGF/VEGF-like factor
Intestinal
tumor growth
PvR
mTOR
Hnf4
mElo
Oenocytes
PC
PE
AcCa
Tracheogenesis